A Volcano Rekindled: The Renewed Eruption of Mount St. Helens, 2004–2006
Edited by David R. Sherrod, William E. Scott, and Peter H. Stauffer
U.S. Geological Survey Professional Paper 1750, 2008

Chapter 26

Emission Rates of CO_2, SO_2, and H_2S, Scrubbing, and Preeruption Excess Volatiles at Mount St. Helens, 2004–2005

By Terrence M. Gerlach[1], Kenneth A. McGee[1], and Michael P. Doukas[1]

Abstract

Airborne surveillance of gas emissions began at Mount St. Helens on September 27, 2004. Reconnaissance measurements—SO_2 column abundances and CO_2, SO_2, and H_2S concentrations—showed neither a gas plume downwind of the volcano nor gas sources within the crater. Subsequent measurements taken during the period of unrest before the eruption began on October 1 and for several days after October 1 showed only small point sources of gas within the crater. These sources defined a pattern of scrubbed degassing that evolved from near-zero emissions, to scattered CO_2-only sources, to growing sources of CO_2 with minor H_2S and SO_2, and finally to myriad sources of CO_2 with increasingly SO_2-dominant sulfur gases. Scrubbing strongly hydrolyzed SO_2 but also affected CO_2 and H_2S.

From October 7 on, a coherent plume spilled over the crater rim, yielding emission rates for CO_2 and SO_2, but not always for H_2S. Virtually all SO_2 and most CO_2 outgassed from the growing dome of new dacite; some CO_2 came from sources on the 1980–86 lava dome and in the Loowit springs area. The 2004–5 emission rates were notably low and variable. Emission rates for CO_2 peaked early (10/7/2004) at 2,415 metric tons per day (t/d), but the median rate was 655 t/d; only about 20 percent of the rates were greater than 1,000 t/d and about 45 percent were less than 500 t/d. Emission rates of SO_2 never exceeded 240 t/d, and the median rate was only 72 t/d; 70 percent of SO_2 emission rates were <100 t/d and about 40 percent were <50 t/d. Emission rates of H_2S were <10 t/d. Cumulative outputs through November 2005 were about 231,000 t CO_2 and 30,000 t SO_2.

The CO_2 and SO_2 emission rates are distinctly lower than those of the early 1980s, but they are similar to those of the 1980s lava-dome eruptions, possibly back as far as late 1981 or late 1980. However, the CO_2/SO_2 ratio of the 2004–5 emissions (11±1) is higher than that of the 1980s emissions (8) because of scrubbing during the early part of the eruption. The nonscrubbed CO_2/SO_2 of the 2004–5 gases is 9±1, similar to the1980s emissions.

Modeling constrained by cumulative CO_2 emissions, cumulative dacite production, and melt H_2O concentration confirms that the 2004–5 dacite is a "flat" magma—that is, a dacite magma greatly depleted in excess (exsolved) volatiles compared to May 18, 1980, dacite. The inferred excess-volatile content of the current dacite is only 1.2 volume percent (vol. percent), or 0.2 weight percent (wt. percent), compared to the 15 vol. percent (3 wt. percent) of the May 18 dacite at 900°C and 220 megapascals (MPa) (8.6 km depth). At the much lower pressure of 130 MPa prior to ascent from the shallowest part of the reservoir (5.2 km depth), the current dacite's inferred excess-volatile content is 1.2 wt. percent—significantly less than the 3 wt. percent of the May 18 dacite and on the low end of the 1–6-wt. percent range of deeper intermediate to silicic magmas commonly involved in explosive volcanism.

The modeling further indicates that before ascent from 5.2 km depth, the dacite's excess volatile phase was H_2O rich (X_{H_2O} = ~0.96, X_{CO_2} = ~0.04, mole fraction basis) with $H_2S/SO_2 > 40$, and its rhyolitic melt phase contained about 4.4 wt. percent H_2O and 37 parts per million (ppm) CO_2. After closed-system ascent to the depth range of groundmass crystallization (~0.5–1 km), X_{H_2O} is 0.98, H_2S/SO_2 is 4–7, and the melt contains 1.1–1.5 wt. percent H_2O and 1–3 ppm CO_2. Sulfur dioxide becomes dominant over H_2S at depths less than 0.2 km. Because of excess-volatile depletion, open-system degassing involves depths shallower than about 2.5 km, weak CO_2 and SO_2 emissions prone to the effects of scrubbing, and—in contrast to early 1980 degassing—no measurable effect on the equilibrium ($^{210}Pb/^{226}$ Ra) values of the 2004–5 dacite.

The 2004–5 gas emissions are incompatible with "new" gas-rich magma introduced into the reservoir in the months

[1] U.S. Geological Survey, 1300 SE Cardinal Court, Vancouver, WA 98683

just before or since the onset of unrest and eruptive activity. However, the gas emissions are compatible with a flat magma—either leftover dacite from 1986 or dacite injected into the reservoir since 1986 as excess volatile-depleted magma, or as gas-rich magma subsequently mixed with larger amounts of leftover dacite or stripped of its excess volatiles by degassing prior to the current eruption.

Introduction

Airborne surveillance of gas emissions began on September 27, 2004, four days after a shallow earthquake swarm beneath the 1980–86 lava dome signaled Mount St. Helens' reawakening after 18 years (Scott and others, this volume, chap. 1; Moran and others, this volume, chap. 2). In this chapter we report the CO_2, SO_2, and H_2S gas emissions from the eruption's inception to the end of 2005, documenting their measurement, sources, and the magnitude and variability of the emission rates—presented in the context of gas-emission rates at Mount St. Helens in the 1980s and at several Cascade Range volcanoes since the late 1990s. The outstanding feature of the 2004–5 gas emissions is their persistently low emission rates. We attribute these low rates mainly to the extreme depletion of excess (that is, exsolved) volatiles in the current dacite compared to the May 18, 1980, dacite and secondarily to gas scrubbing. VolatileCalc modeling (Newman and Lowenstern, 2002) quantifies and confirms our hypothesis of excess-volatile depletion in the 2004–5 dacite. We exploit the modeling to reveal the amount and composition of excess-volatile fluid in the source dacite at depth, to track its evolution as the dacite ascends, and to quantify several related aspects of the degassing.

Background

Airborne Emission-Rate Measurements at Mount St. Helens in the 1980s

Airborne monitoring from a fixed-wing aircraft of SO_2 emission rates began at Mount St. Helens in May 1980 by making correlation spectrometer (COSPEC) measurements on the plume. More than 1,000 COSPEC flights followed during the next 8 years (McGee, 1992; McGee and Casadevall, 1994), most of which were made 1–2 km downwind of source vents during episodes of dome-building eruptions, endogenous dome growth, or intervening noneruptive periods. Casadevall and others (1981, 1983) describe the measurement technique and discuss the SO_2 emissions through 1982. McGee (1992) describes the structure, dynamics, and SO_2 cross sections of noneruptive plumes at Mount St. Helens that occurred from 1980 to 1988. McGee and Sutton (1994) discuss measurements made during four 1984–86 dome-building eruptions and compare results with various geophysical monitoring data. Early SO_2 emission rates frequently exceeded 1,000 metric tons per day (t/d), but rates declined to negligible levels by September 1988 when airborne COSPEC measurements ended, nearly 2 years after the last dome-building eruption of the 1980s (McGee and Casadevall, 1994). Airborne monitoring also included 119 measurements of CO_2 emission rates that ranged from >20,000 t/d in July 1980 to <1,000 t/d by the end of August 1981, when measurements were halted because concentrations of plume CO_2 had declined to levels indistinguishable from ambient atmospheric CO_2 by the analyzer employed at the time (Harris and others, 1981; McGee and Casadevall, 1994). McGee and Casadevall (1994) tabulate the 1980–1988 airborne emission-rate measurements and supplementary data, all of which can be downloaded from the USGS publications Web site, http://pubs.usgs.gov/of/1994/of94-212/ (last accessed March 14, 2008).

Airborne Emission-Rate Measurements in the Cascades Since the 1980s

We initiated a program of volcanic gas emission-rate measurements at Cascade Range volcanoes in the late 1990s after developing improved airborne monitoring techniques (described below). The program comprised airborne plume measurements at major volcanic centers, from Mount Baker in Washington to Lassen Peak in California, to establish baseline emission rates of CO_2, SO_2, and H_2S for identifying anomalous gas emissions at times of volcano unrest in the Cascade Range (table 1). Several volcanic centers—Glacier Peak, Mount Rainer, Mount Adams, Mount Jefferson, Medicine Lake caldera and Mount Shasta—produce no detectable emissions of the three gases; however, these airborne results do not rule out minor diffusive degassing and scattered spring and fumarole gas discharges derived from underlying magma. Other centers, such as Newberry caldera and South Sister, though lacking coherent plumes, do produce trace quantities of gas from small point sources that can be detected in airborne gas measurements. Besides Mount St. Helens, only three volcanoes in the Cascade Range produce coherent plumes with measurable gas output at the present time—Mount Baker, Mount Hood, and Lassen Peak. All of these volcanoes emit small amounts of gas: emission rates are <300 t/d for CO_2 and <10 t/d for H_2S; SO_2 is below detection.

Airborne Measurements at Mount St. Helens in 1998

In May 1998, background seismicity at Mount St. Helens increased markedly from the low levels recorded for the previous few years. Located directly below the lava dome, these small earthquakes clustered mainly in two distinct depth bands: 2–5 km and 7–9 km. Throughout June and the first half of July 1998, the seismicity continued to increase, with earthquake depths spanning the entire range from 2 to 9 km. The first of several airborne gas-surveillance flights recorded

Table 1. Gas measurements in the Cascade Range and nearby calderas after 1988.

[Platform indicates aircraft: FX, fixed-wing; Heli, helicopter. t/d, metric tons per day; –, no data; 0, measurement taken but gas was not detected; tr, trace.]

Volcano	Date	Platform	CO_2 (t/d)	SO_2 (t/d)	H_2S (t/d)
Mount Baker	07/08/1998	FX	273	0	–
	09/13/2000[1]	FX	187	0	5.5
	03/21/2001	FX	0	0	0
Glacier Peak	07/08/1998	FX	0	0	–
Mount Rainer	07/08/1998	FX	0	0	–
Mount Adams	08/03/1998	FX	0	0	–
	08/10/2005	FX	0	0	0
Mount St. Helens	06/22/1998	FX	1,900	0	–
	07/08/1998[2]	FX	tr	0	–
	07/08/1998[3]	FX	tr	0	–
	08/03/1998	FX	0	0	–
	09/14/1998	FX	0	0	–
Mount Hood	06/22/1998	FX	0	0	–
	08/03/1998	FX	0	0	–
	08/10/2005	FX	0	0	0
	09/15/2005	Heli	144	0	6.4
Mount Jefferson	08/11/1998	FX	0	0	–
Newberry caldera	09/19/2000	FX	tr	0	–
South Sister	04/25/2001	Heli	tr	0	–
	09/21/2001	Heli	0	0	–
Medicine Lake caldera	08/11/1998	FX	0	0	–
Mount Shasta	08/11/1998	FX	0	0	–
Lassen Peak	08/11/1998	FX	110	0	–
	09/19/2000	FX	20	0	2

[1]Data from McGee and others (2001).

[2]Morning flight.

[3]Afternoon flight.

a CO_2 emission rate of 1,900 t/d on June 22 (table 1). By July 8, morning and afternoon gas-measurement flights detected only trace CO_2 degassing, and by the end of July, seismicity returned to levels similar to those prior to May. Additional gas-surveillance flights on August 3 and September 14 failed to detect CO_2 degassing. All 1998 flights failed to detect SO_2; there were no H_2S measurements.

Instrumentation and Configuration of the Airborne Monitoring System

In this study, we used an airborne system developed during the past decade for measuring volcanic CO_2, SO_2, and H_2S emissions and intended primarily for application in the Cascade Range and the Aleutian arc. Sites of interest in these regions are remote, ground access is difficult, climates are wet, and thick snow pack and glaciers are present locally. Large volumes of recharge water foster hydrothermal systems and bodies of ground water and surficial water capable of scrubbing acidic magmatic volatiles (especially SO_2, HCl, HF) and masking magma degassing at depth during the early stages of unrest—hence the emphasis on an airborne system capable of measuring CO_2 and H_2S emissions (Doukas and Gerlach, 1995; Symonds and others, 2001).

The airborne system incorporates a LI-COR Model LI-6252 nondispersive infrared CO_2 analyzer and flow control unit to measure CO_2 concentrations. This instrument, with a fast 1-s response time and a high sensitivity to low concentrations of CO_2, is well suited for measuring small changes in CO_2 concentration. Its use for determining CO_2 in volcanic plumes is described in detail elsewhere (Gerlach and others, 1997; Gerlach and others, 1999). We used an Interscan Model 4170 H_2S analyzer to measure plume H_2S in the 0–1 ppm range. This instrument consists of an electrochemical voltametric sensor coupled to a 1-L/min sample-draw pump with H_2S concentration recorded from calibrated analog output. McGee and others (2001) describe the application of the Interscan analyzer to measuring H_2S in volcanic plumes. Similarly, an Interscan Model 4240 SO_2 analyzer with a 0–2 ppm range provides direct measurements of SO_2 in the plume. Assuming ambient air is largely devoid of H_2S and SO_2, our measurements indicate typical instrument noise values of 3–4 parts per billion (ppb)for these analyzers. Interscan analyzers show some cross sensitivity to other gases, so these gases are removed by appropriate chemical scrubbers installed on input lines. Because Interscan analyzers measure gas partial pressures, all calibrated output is corrected for the pressure and temperature at the altitude of measurement.

The airborne system is configured to employ two types of optical ultraviolet spectrometers for measuring SO_2 column abundances. For some of the early measurements in this study, we employed a Barringer correlation spectrometer (COSPEC V)—long the standard tool for monitoring volcanic SO_2 emission rates (Stoiber and Jepsen, 1973; Crafford, 1975; Malinconico, 1979; Stoiber and others, 1983). A data logger records the analog output of the instrument for later processing using USGS software. For the majority of the SO_2 flux measurements, we used a FLYSPEC built and configured as described in Horton and others (2006). This new, miniaturized, lightweight and low-power, ultraviolet correlation spectrometer incorporates an Ocean Optics USB2000 ultraviolet spectrometer with a fiber-optic collimating lens, a UV band-pass filter, and two SO_2 calibration cells. A subnotebook computer provides FLYSPEC power, control, and data collection through a USB port, and a small GPS receiver supplies location data for cosine corrections of traverses not perpendicular to the direction of plume travel.

The airborne instrument package also includes a type-K thermocouple, shielded from wind and direct sunlight, for measuring ambient air temperature and a chart recorder for in-flight logistical use. A pressure transducer mounted within the LI-COR analyzer provides measurements of ambient atmospheric pressure inside the unpressurized aircraft cabin. An onboard Rockwell GPS receiver continuously records the precise latitude, longitude, and altitude, so that the location of each measurement can be retrieved later for data processing. The data from all instruments except the FLYSPEC are recorded at 1-s frequency in a handheld PSC Falcon Model 310 portable data-collection terminal. Figure 1 illustrates schematically the configuration of all the instruments of the airborne system. Figure 2 displays instrument placement in both helicopter and fixed-wing aircraft and the external helicopter mounting of a FLYSPEC.

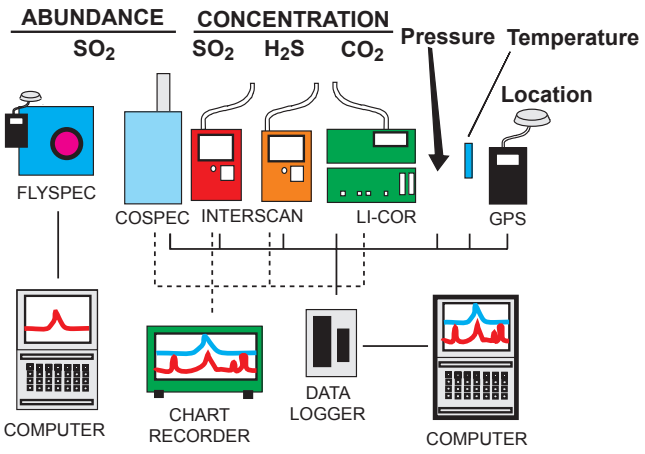

Figure 1. Airborne instrument package showing instruments used for measuring SO_2 column abundances (FLYSPEC and COSPEC); instruments for measuring CO_2, SO_2, and H_2S gas concentration (LI-COR and Interscan); sensors for measuring temperature, pressure, and location; and other components used during a typical airborne mission (computer, data logger, and chart recorder).

Procedures and Methods

The gas measurements began on September 27, 2004. The five flights during the first week were primarily for reconnaissance purposes. At this stage of unrest, the volcano lacked a coherent gas plume but produced small fragmentary and ephemeral parcels of gas that—although detectable by the airborne system—were only useful for rough estimates of gas emission rates. Nevertheless, we were able to discover and follow the development of point sources of emerging gas emissions within the crater by mounting the direct-sampling instruments (LI-COR and Interscans) in a helicopter with an air intake tube attached to the lower left strut and making reconnaissance flights of the 1980–86 lava dome, the crater floor, and the crater walls (fig. 3).

After the first week of October 2004, a coherent plume developed and spilled over the crater rim, and accurate emission-rate determinations became feasible (fig. 4). We mounted and flew the direct-sampling instruments and the COSPEC V in a twin-engine aircraft configured for open-flow sampling of external air (Gerlach and others, 1997, 1999). The use of a twin-engine aircraft prevented contamination by combustion products from engine exhaust. Upward-looking COSPEC measurements taken while flying traverses beneath the plume perpendicular to the direction of plume transport provided SO_2 column abundances across an orthogonal section of the plume (fig. 5*A*). Flying traverses across the plume at different altitudes, each normal to its transport direction, allowed in-plume measurements and profiling of entire orthogonal sections of the plume by the direct-sampling instruments (LI-COR and Interscans) (fig. 5*B*). Figure 6 illustrates a series of airborne traverses across the plume, showing where the Interscan analyzer detected SO_2 in the orthogonal plume cross section. Later processing of these data into emission rates included corrections for curvature in the flight paths and for deviations from orthogonality. Contour maps of gas concentrations in the orthogonal plume cross section were produced using mapping software (Surfer v. 8).

By November 10, 2004, we made a transition to the use of a helicopter as the airborne platform for gas measurements, for these reasons: the availability of a helicopter for field work, the superior maneuverability of a helicopter for making plume measurements at the crater rim and within the crater, and the slower airspeed of the helicopter, which permits more measurements per meter across small plumes. Use of the helicop-

Figure 2. Gas-monitoring equipment installation for airborne surveillance, 2004–2005. *A*, FLYSPEC being attached to the strut of helicopter. The instrument's narrow field of view allows it to be mounted near the body of the aircraft without blocking the light. *B*, Typical mounting arrangement of instrumentation in helicopter. *C*, Instrumentation placed in a fixed-wing aircraft. Note COSPEC panel (right) protruding from behind copilot's seat. USGS photos by K.A. McGee (*A*, *C*) and M.P. Doukas (*B*).

ter also marked the transition to exclusive use of the FLYSPEC ultraviolet spectrometer for SO_2 emission-rate measurements. Although it is possible to utilize the COSPEC in a helicopter, "chopping" of light to the COSPEC telescope by the rotor blades creates interference in the signal output. This requires selection of longer time constants to dampen the interference, which negates the advantageous spatial resolution of the helicopter (Caltabiano and others, 1992; Galle and others, 2002; Elias and others, 2006). The FLYSPEC, however, is relatively immune to interference by the rotor blades, and no special filtering or processing of the data is required. The switch from COSPEC to FLYSPEC did not introduce inconsistencies into the SO_2 emission-rate dataset—side-by-side testing of these instruments shows they produce statistically equivalent results (Elias and others, 2006; Horton and others, 2006).

The relatively small field of view (2.5°) of the FLYSPEC allows it to be mounted on an external structural member close to the body of the helicopter and positioned to point vertically without loss of signal due to light obstruction (fig. 2*A*). We fed the USB signal and power cable through a side window of the helicopter to connect with the subnotebook computer. Prior to the plume measurements, we landed the helicopter at a calibration station high on the flank of Mount St. Helens and collected instrument spectra for the high and low calibration cells along with spectra for dark current and clear sky. Once the FLYSPEC was calibrated, we flew several traverses beneath the plume that were averaged to obtain the SO_2 column abundances of the plume. We reduced the data with the FluxCalc software program written by staff at the Hawai'i Institute of Geophysics and Planetology, University of Hawai'i at Mānoa. The program compares absorption values of as many as nine peak-and-trough combinations in each sample SO_2 spectrum to the two calibration cell spectra and then computes the column abundance of SO_2.

The standard method for determining emission rates from airborne in-plume measurements by the direct-sampling instruments is based on the volcanic gas concentrations measured in the cross section through the plume normal to wind direction, the average plume pressure and temperature in that section, and the wind speed (Harris and others, 1981; Gerlach and others, 1997). Gerlach and others (1999) adapted the method by using orbital traverses around a volcano and correcting the data from curved plume cross sections approximately normal to wind direction. McGee and others (2001) further adapted the method by using H_2S peaks as a guide for resolving the boundary between atmospheric-only CO_2 and atmospheric plus volcanic plume CO_2. In this study, we often used the location of SO_2 peaks recorded by the Inter-scan analyzer as markers to distinguish plume CO_2 from the atmospheric background CO_2 because H_2S was not always detected in the plume. Direct measurement of CO_2 and SO_2

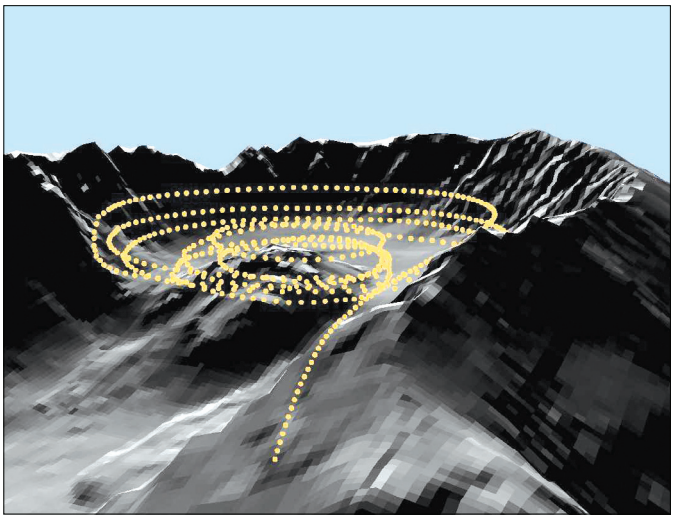

Figure 3. Shaded-relief elevation model of Mount St. Helens' crater indicating the flight path of a gas-measurement flight in October 2004. Early gas flights in fall 2004 before the emergence of a discrete plume, such as the flight illustrated here, were geared toward detecting point sources of CO_2, SO_2, and H_2S. View is to the southeast.

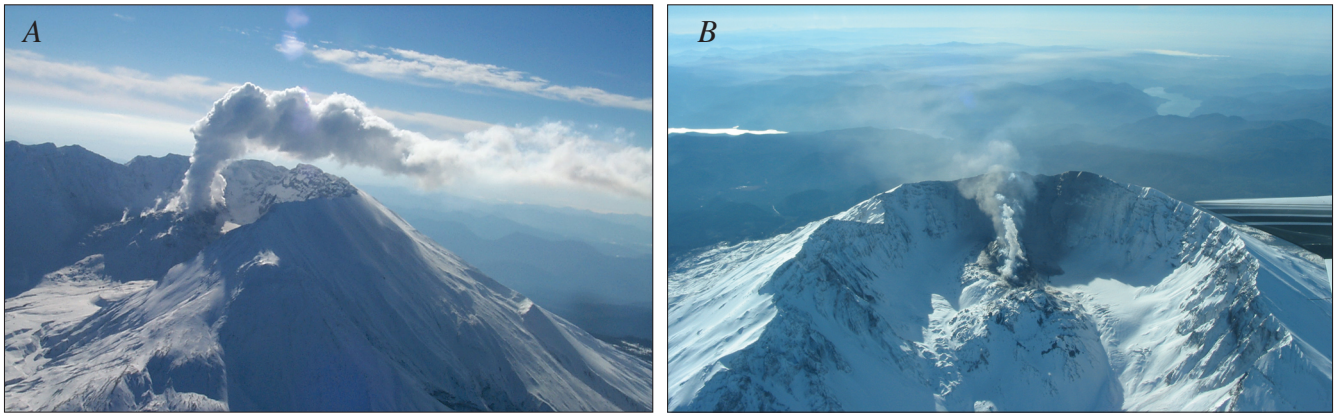

Figure 4. Typical gas plumes from Mount St. Helens early in the 2004–2005 eruption. *A*, Plume observed on October 27, 2004. View is to southeast. *B*, Plume on November 4, 2004. View is to south. Crater diameter is about 2.1 km.
USGS photos by M.P. Doukas (*A*) and K.A. McGee (*B*).

also allowed calculation of CO_2/SO_2 ratios at many locations in the plume.

Knowing the velocity of plume travel is essential in computing accurate gas-emission rates from either gas concentrations in a plume cross section or column-abundance measurements made beneath the plume. It is assumed that the speed of the plume as it moves downwind is the same as the ambient wind speed. We used the Doukas (2002) method of wind-speed measurement, in which a GPS receiver records the rate and direction of drift of the aircraft while flying neutral wind circles at the altitude of the plume. This information allows determination of wind speed and wind direction at the altitude of the plume with a windspeed uncertainty of <10 percent.

The equation of Gerlach and others (1997),

$$E_{CO_2} = 0.457329(ASP_{CO_2})/T, \quad (1)$$

calculates the CO_2 emission rate, E_{CO_2}, in t/d where A is the area of the plume cross section after corrections for curvature of orbital traverses (in m^2), S is the average plume speed (in m/s), P_{CO_2} is the average partial pressure of CO_2 in the plume (in pascals (Pa), calculated from the product of average barometric pressure in the plume and the average mole fraction concentration of CO_2 in the plume), and T is the average air temperature in the plume (in K). The constant (units: s t K Pa^{-1} m^{-3} d^{-1}) includes the kilogram molecular weight of CO_2 (0.04401 kg/mol), the universal gas constant (8.314510 Pa m^3 mol^{-1} K^{-1}), and the conversion factors 86,400 s/d and 10^3 kg/t. When calculating E_{H_2S}, P_{CO_2} is replaced by P_{H_2S}, and the con-

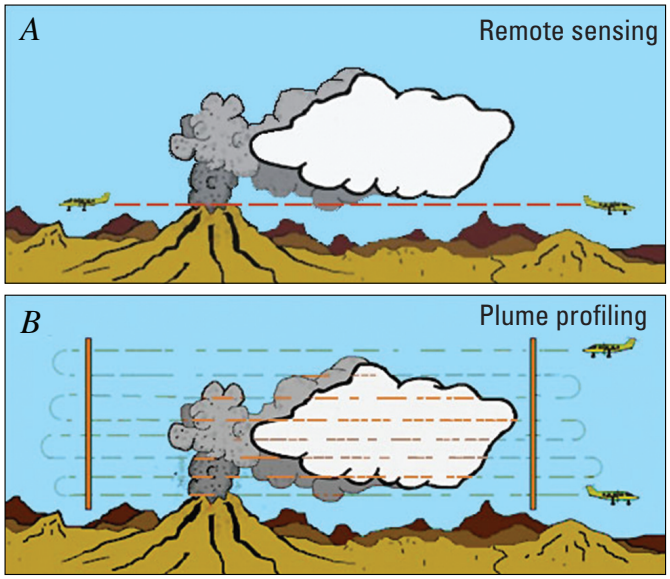

Figure 5. Schematic flight patterns for plume monitoring. *A*, Flight pattern for remote measurement of SO_2 column abundances in the plume. Flight traverses with the upward-looking FLYSPEC or COSPEC spectrometer are made beneath the plume perpendicular to its direction of travel. *B*, Instruments that measure concentration and require direct sampling of the plume, such as LI-COR and Interscan, are flown directly through the plume, perpendicular to its travel direction, in a series of top-to-bottom profiles forming a vertical plume cross section.

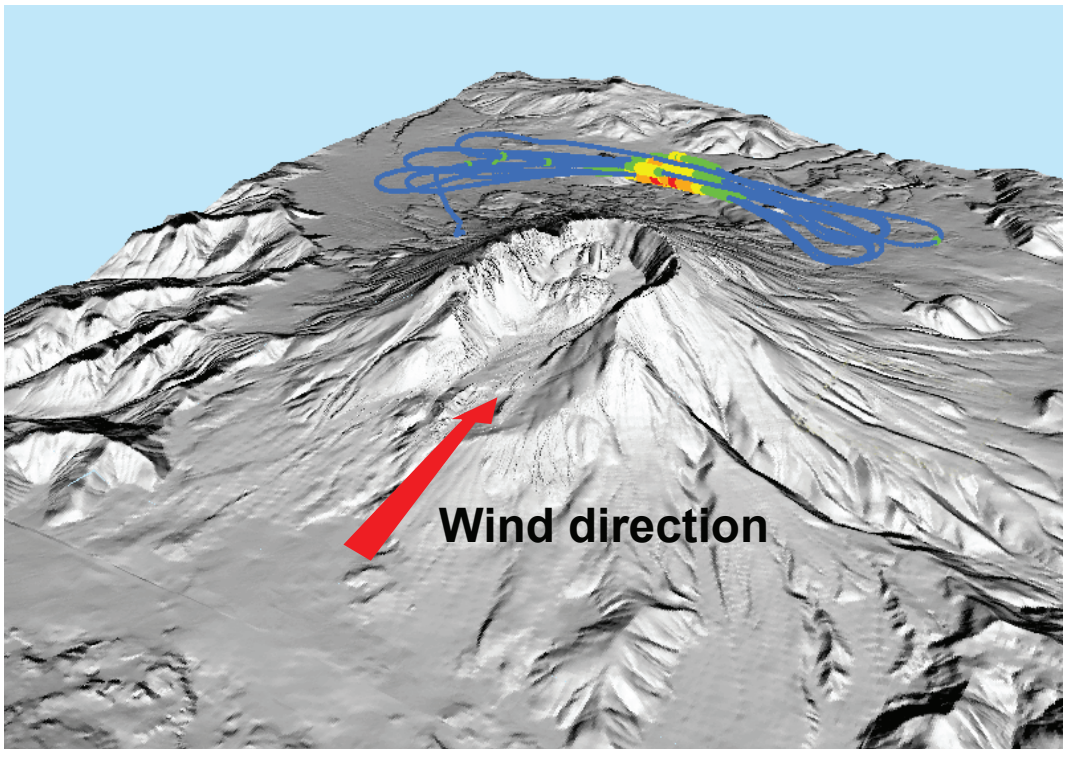

Figure 6. Illustration of a downwind airborne measurement of the plume from Mount St. Helens on July 13, 2005, plotted on shaded-relief elevation model. View is to the southeast. Blue line represents GPS tracks of several traverses through the plume, with hotter colors (yellow, orange, and red) representing locations where SO_2 was measured. Red arrow indicates wind direction; wind is from the north.

stant is 0.354141 (McGee and others, 2001); when calculating E_{SO_2}, P_{SO_2} and the constant 0.665665 are used.

Flight frequency varied because of a mix of factors, which included perceived flight safety, apparent necessity of the data for hazard assessments, rate of change of eruptive activity, and current and forecasted weather. Starting on September 27, 2004, we made 11 flights in the first 3 weeks, 1 to 2 flights per week during the next 5 weeks, and 1 or 2 flights per month thereafter throughout 2005, except during December 2005 when weather conditions did not permit access to the plume. Flight dates and aircraft platforms deployed (helicopter or fixed-wing) are recorded in table 2.

Description of Data and Statistical Tests

Gas emission-rate data, which form the backbone data of this report, tend to have skewed rather than symmetrical distributions. The skewed distributions are a reflection of two fundamental properties of gas emission-rate data: they can take on only positive values, and their standard deviations are typically large—commonly about as large or larger than their means. When distributions are skewed, means and standard deviations may no longer adequately describe population distributions, and interpreting these statistics in terms of a normal distribution can produce a misleading picture. It is preferable instead to report the median for skewed distributions (Glantz, 2005); we also report upper and lower percentile information as appropriate to give an indication of the dispersion of values in the sampled population.

If populations are skewed from normal distributions, parametric statistical tests may become unreliable, and nonparametric or distribution-free statistical tests should be used (Glantz, 2005). Therefore, we used statistical software (SigmaStat v. 3.1) to calculate the nonparametric Mann-Whitney rank-sum test (MWRST), instead of the parametric Student's *t* test, to test for significant differences in two groups of data. The MWRST can be used to evaluate significant difference in the medians of two groups, significant difference in the underlying population distributions of two groups, and significant difference between two groups caused by random sampling variations. We report the probability level (*P*) of MWRST results. Following the tradition of most physical-science research, the critical significance level for *P* is 5 percent ($P = 0.05$) in this report; that is, $P \leq 0.05$ indicates a significant difference. Several of the statistical calculations also included Kolmogorov-Smirnov normality testing (SigmaStat v. 3.1).

Results and Observations

Emission Rates, Cumulative Emissions, and CO_2/SO_2 Ratios

The measured CO_2, SO_2, and H_2S emission rates of the 2004–5 eruption spanned the period from September 27, 2004, to November 22, 2005 (fig. 7, table 2). Emission rates frequently were below detection limits before October 7, 2004 (fig. 7, table 2). Time series of the 24 CO_2 and 28 SO_2 emission rates measured from October 7, 2004, until the last 2005 measurement on November 22 were notably low and variable. Emission rates ranged from 2,415 t/d to 146 t/d for CO_2 and from 240 t/d to 14 t/d for SO_2; both CO_2 and SO_2 had low medians: 655 t/d for CO_2 and 72 t/d for SO_2. Less than 5 percent of the CO_2 emission rates were >2,000 t/d, about 80 percent were <1,000 t/d, more than 40 percent were <500 t/d, and about 25 percent were <250 t/d. Of the SO_2 emission rates, only 7 percent were >200 t/d, almost 70 percent were <100 t/d, and 40 percent were <50 t/d. At times, emission rates fell to <150 t/d for CO_2 and to <30 t/d for SO_2. Emission rates of H_2S were always low (<10 t/d). Multiple traverses under the plume gave comparable SO_2 emission rates, so the observed variation was not simply from puffing during times of measurement.[2]

Cumulative CO_2 and SO_2 emissions—calculated from the areas under emission-rate time-series plots—indicate total outputs of 231,150 t CO_2 and 29,700 t SO_2 from October 7, 2004, through November 22, 2005 (fig. 8; table 2). Weighted emission rates—calculated from cumulative emissions on measurement dates (fig. 8; table 2) divided by the number of days since October 7, 2004—are like multiday averages and thus smoother than measured emission rates. Although less variable, weighted emission rates also have low medians—830 t/d for CO_2 and 99 t/d for SO_2. However, these median rates are somewhat higher than the medians of measured values. Nevertheless, statistical tests confirm that no significant dif-

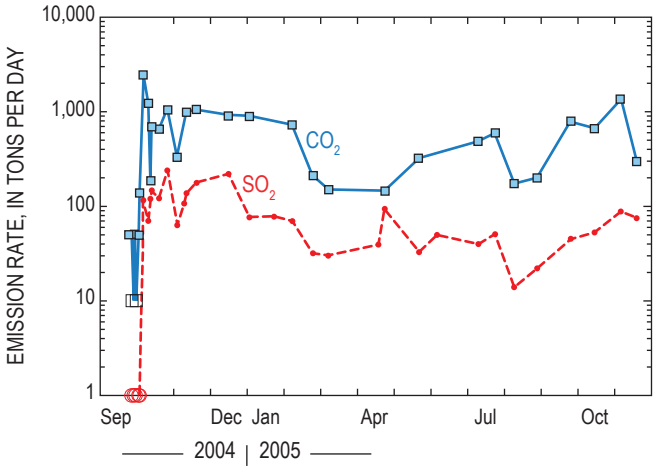

Figure 7. Time-series plots of CO_2 and SO_2 emission rates from September 27, 2004, to November 22, 2005 (table 2). The open symbols for some earlier measurements between September 27 and October 1, 2004, indicate estimated detection limit values of 10 t/d (CO_2) and 1 t/d (SO_2).

[2] Note added in proof: Low emission rates of 150–300 t/d CO_2, 5–35 t/d SO_2, and < 0.1 t/d H_2S persisted during 12 gas-monitoring flights from 2006 until the eruption paused in late January 2008.

Table 2. Emission rates and cumulative emissions for CO_2, SO_2, and H_2S during 2004–2005, Mount St. Helens, Washington.

[Emission rates are measured rates used in calculations of this study; significant figures were exaggerated to reduce roundoff errors. Cumulative emissions were determined as described in the text. Platform indicates aircraft: FX, fixed-wing; Heli, helicopter. t/d, metric tons per day; nd, not determined.]

Date	Platform	CO_2 (t/d)	SO_2 (t/d)	H_2S (t/d)	CO_2 (t)	SO_2 (t)
09/27/2004	Heli	50	1 [1]	0.1 [1]	nd	nd
09/29/2004	Heli	10 [1]	1 [1]	0.1 [1]	nd	nd
09/30/2004	Heli	50	1 [1]	0.1 [1]	nd	nd
10/01/2004	Heli	10 [1]	1 [1]	0.1 [1]	nd	nd
10/03/2004	Heli	50	1 [1]	0.1 [1]	nd	nd
10/04/2004	Heli	140	1 [1]	0.4	nd	nd
10/07/2004	FX	2,415	115	8	2,415	115
10/11/2004	FX	1,222	70	4	7,274	370
10/13/2004	FX	186	120	6	8,682	560
10/14/2004	FX	710	148	0.1 [1]	9,130	694
10/20/2004	FX	652	121	8	13,216	1,501
10/27/2004	Heli	1,060	240	8	19,208	2,764
11/04/2004	FX	332	63	0.1 [1]	24,776	3,976
11/10/2004	Heli	nd	107	6	nd	4,486
11/12/2004	Heli	981	138	nd	30,028	4,732
11/20/2004	Heli	1,053	177	6	38,164	5,993
12/17/2004	Heli	914	221	5	64,718	11,370
01/03/2005	Heli	887	76	0.1 [1]	80,027	13,893
01/24/2005	Heli	nd	78	11	nd	15,509
02/08/2005	Heli	718	70	0.3	108,917	16,619
02/25/2005	Heli	211	32	0.6	116,814	17,485
03/10/2005	Heli	149	30	0.3	119,154	17,888
04/21/2005	Heli	nd	40	0	nd	19,347
04/26/2005	Heli	146	94	0	126,086	19,681
05/25/2005	Heli	325	33	0	132,916	21,522
06/09/2005	Heli	nd	50	nd	nd	22,145
07/13/2005	Heli	485	40	nd	152,760	23,675
07/27/2005	Heli	594.3	51	0.1 [1]	160,316	24,312
08/12/2005	Heli	174	14	0.1 [1]	166,462	24,832
08/31/2005	Heli	198	22	0.1 [1]	169,996	25,174
09/28/2005	Heli	789	45	0.1 [1]	183,814	26,112
10/18/2005	Heli	658	53	0.3	198,284	27,092
11/09/2005	Heli	1,353	88	0.1 [1]	220,405	28,643
11/22/2005	Heli	300	75	0.1 [1]	231,150	29,702

[1]Estimated detection limits for CO_2, SO_2, and H_2S emission rates.

ference exists between the medians of measured and weighted CO_2 and SO_2 emission rates and the populations they sample (P >0.05).

The 24 contemporaneous CO_2 and SO_2 emission rates measured from October 7, 2004, to November 22, 2005, have a median molar CO_2/SO_2 ratio of ~12; about half of the CO_2/SO_2 ratios are between 7 and 18. The corresponding weighted emission rates have a median CO_2/SO_2 of ~10 and about half the CO_2/SO_2 ratios are between 9 and 11. Statistical tests confirm there is no significant difference between CO_2/SO_2 ratios calculated from measured and weighted emission rates (P >0.05). Total emissions for the entire period—231,150 t CO_2 and 29,700 t SO_2—indicate a CO_2/SO_2 of ~11. Thus, we employ a grand median CO_2/SO_2 ratio of 11±1 in this report.

Early Degassing

From the start of airborne gas measurements on September 27, 2004, throughout the period of unrest before the eruption began on October 1 and for almost a week thereafter, a volcanic plume was either absent or present as small fragmentary and ephemeral parcels of gas, yielding only rough gas-emission rates (table 2). Flights during this period served mainly as reconnaissance surveys for gas-emitting sources on the 1980–86 dome, the crater floor, and the crater walls (fig. 3) and led to the discovery and observation of point sources of gas emission that, over time, established a record of emergent degassing. The record began with SO_2 and H_2S concentrations at detection limits at all locations and CO_2 concentrations at ambient atmospheric levels at most locations (fig. 9), although sporadic CO_2 sources occurred with minor peaks <1.5 ppm above ambient levels. Similar results persisted through September 30. After the first steam-and-ash explosion at the start of the eruption on October 1, new CO_2 concentration peaks above ambient levels appeared—one new source on the northwest face of the 1980s dome produced an above-background peak of 36 ppm—but SO_2 and H_2S still remained largely at noise levels. There was some evidence, however, of the presence of H_2S—one minor peak was observed, and some observers in the air and on the ground downwind of the volcano reported the odor of H_2S.

The number of fumarole sources increased significantly by October 2, as did the number of above-ambient CO_2 concentration peaks—one reaching up to 16 ppm—while SO_2 and H_2S continued to be mostly absent, although field crews again reported H_2S odors (fig. 10). A further increase in the number of fumaroles and a broadening of CO_2 anomalies along with coincident low H_2S peaks (<0.02 ppm) appeared in the record on October 3. By October 4, CO_2 anomalies were as broad as a kilometer or more across, and SO_2 and H_2S formed coinci-

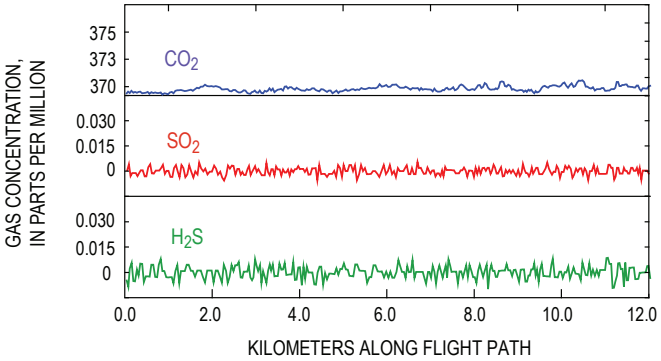

Figure 9. Concentrations of CO_2, SO_2, and H_2S measured along a helicopter flight path in Mount St. Helens crater on September 27, 2004. Concentrations of CO_2 are similar to ambient atmospheric levels; concentrations of SO_2 and H_2S are at sensor detection limits.

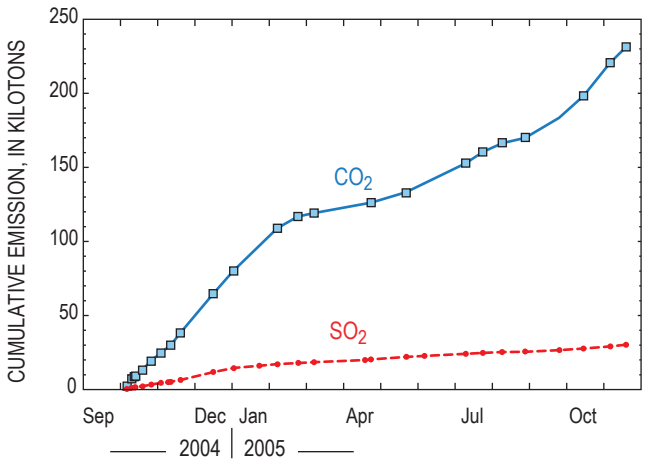

Figure 8. Time-series plots of cumulative CO_2 and SO_2 emissions from October 7, 2004, to November 22, 2005, when emission rates for both gases were above detection limits (fig. 7; table 2).

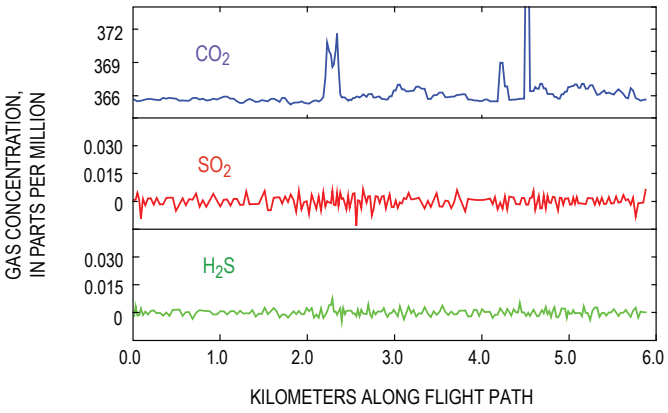

Figure 10. Concentrations of CO_2, SO_2, and H_2S measured along a helicopter flight path in Mount St. Helens crater on October 2, 2004. Concentrations of CO_2 show sporadic spikes above ambient atmospheric levels; concentrations of SO_2 and H_2S remain at sensor detection limits. The clipped CO_2 peak rises to 382 ppm.

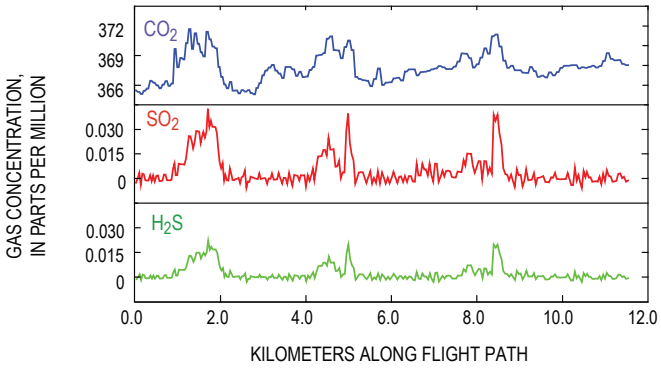

Figure 11. Concentrations of CO_2, SO_2, and H_2S measured along a helicopter flight path in Mount St. Helens crater on October 4, 2004. Concentrations of CO_2 show broad anomalies above ambient atmospheric levels; concentrations of SO_2 and H_2S show sharply coincident anomalies spiking above sensor detection limits. Note that SO_2 and H_2S anomalies have concentration levels of roughly similar magnitude.

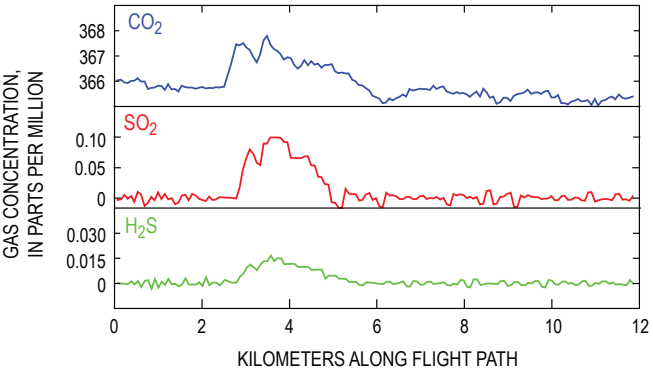

Figure 12. Concentrations of CO_2, SO_2, and H_2S measured along a helicopter flight path in Mount St. Helens crater on October 11, 2004. Concentrations of CO_2 show a broad anomaly above ambient atmospheric levels; concentrations of SO_2 and H_2S show coincident anomalies. Note that concentration levels of the SO_2 anomaly now are clearly greater than those of H_2S.

dent anomalies of roughly equivalent concentration levels (fig. 11). Wet degassing prevailed at this time as large gas bubbles were seen streaming through and ejecting from pools of water, which often contained chunks of floating ice that calved in from the adjacent melting glacier. By October 11, SO_2 clearly dominated H_2S as temperatures rose, pools of water dried up, and steaming increased greatly (fig. 12). Coherent plumes began to form regularly on or about October 7 and spilled over the crater rim (fig. 4), permitting acquisition of reliable emission rates by remote SO_2 column-abundance measurements and direct measurements of CO_2, SO_2, and H_2S gas concentrations (fig. 13).

Composite Degassing Sources

Mount St. Helens continued to produce buoyant plumes throughout the remainder of 2004 and all of 2005. In addition to the principal degassing site from the vent area on the north side of the new dome, several additional sites degassing both CO_2 and SO_2 were present at various locations on both old and new lobes of the growing new dome. By summer 2005, gas emissions were declining, and airborne gas measurements began to be conducted closer to the gas sources. These measurements provided more spatial resolution of gas concentrations within the proximal plume and revealed a minor source of the CO_2 within the plume coming from the 1980s dome. Since 2005, we have consistently detected CO_2 coming from the southwest side of the 1980s dome, just north of the vent area for the new dome. In addition, the older dome hosts a smaller CO_2 source on its east shoulder and several scattered point sources of CO_2. The spatial separation of new-dome and old-dome gas sources is best developed when winds are from the east or west. The degassing from the 1980s dome involves little or no SO_2. Nearly all of the SO_2 in the plume, and the majority of CO_2, originates from the hotter vents associated with the new dome. Under appropriate wind conditions, airborne traverses through the plume show CO_2 clearly degassing from both domes, whereas SO_2 is virtually absent from the

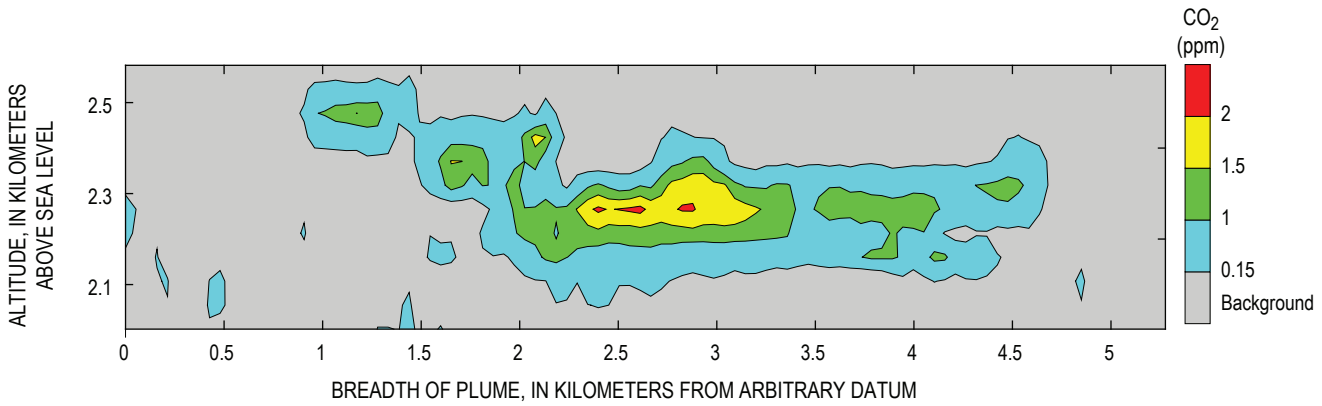

Figure 13. Concentrations of CO_2 in a vertical cross section of a coherent gas plume from Mount St. Helens on November 12, 2004, 1.7 km downwind of source. Bar on right shows scale for concentration of CO_2 above local atmospheric background. Plume cross section gives a CO_2 emission rate of 980 t/d.

1980s dome (fig. 14). Figure 14 shows CO_2 concentrations on a single plume traverse; most plume traverses show CO_2 concentrations are much higher over the new dome.

CO_2 Plume from Loowit Springs

During some of the airborne gas-measurement flights, a small CO_2 plume was observed that did not emanate from the new or the old dome. The source of this plume proved to be the Loowit springs area (Thompson, 1990), north of the 1980s dome and near the mouth of the crater, as determined by a series of low helicopter traverses on June 9, 2005, when winds from the north or northwest were favorable for distinguishing it. Orbital profiling around the upper part of the Loowit drainage defined the extent of the plume and quantified the CO_2 emission rate at 27 t/d (fig. 15), although the exact spring or springs involved could not be distinguished; neither SO_2 nor H_2S were detected. The spring discharge of magmatic CO_2 as inorganic carbon (aqueous CO_2 and HCO_3^- in about equal amounts) dissolved in Loowit waters and other thermal features draining the crater is ~22 t/d, which is similar to the emission rate of CO_2 gas around Loowit (Bergfeld and others, this volume, chap. 25). It is not known if the Loowit springs plume is a result of the current eruption or a longer-term feature.

Discussion

The key fact about the CO_2 and SO_2 emission rates is that they are generally low. This fact was evident early on and motivated our hypothesis that the CO_2 and SO_2 emissions of the 2004–5 eruption were derived from source dacite depleted in excess (that is, exsolved) volatiles at depth (Gerlach and others, 2005), herein termed "flat" magma. The corollary hypothesis—that gas emissions from flat dacite are expressly vulnerable to scrubbing, particularly during the unrest and early stages of the eruption—follows from the depletion in excess volatiles. The flat magma and gas scrubbing hypotheses underlie much of the discussion that follows.

Comparisons with 1980s Emission Rates

Comparisons of the 1980s and 2004–5 passive emission rates of SO_2 and CO_2 support the interpretation that the current eruption involves flat magma, possibly left over in the reservoir since the last lava-dome eruption in 1986. The 2004–5 SO_2 emission rates (fig. 7; table 2) are not significantly different from 1980s SO_2 emission rates during the period from October 18, 1980, to December 9, 1986 (fig. 16), according to the MWRST ($P \geq 0.05$). This time interval matches closely

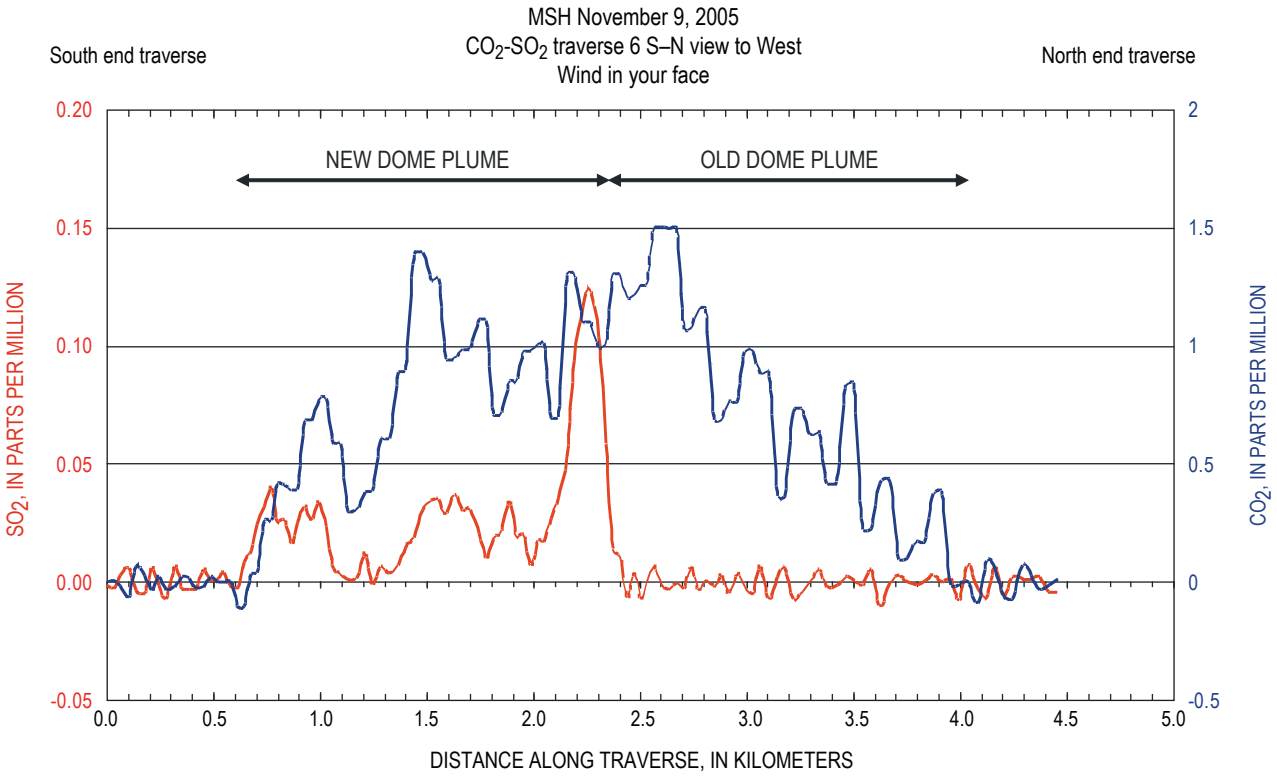

Figure 14. Airborne traverse of plume on November 9, 2005, showing above-background CO_2 concentration (blue) and SO_2 concentration (red). Wind direction from nearly due west allows comparison of plume data from the new dome complex with the older 1980–1986 dome. Traverse flown approximately 2.3 km downwind of central source area. The older dome is discharging CO_2 but little or no SO_2.

the period of 17 lava-dome eruptions and stable dome growth that produced the 1980s dome. October 18, 1980, is the date of the first SO_2 emission-rate measurement after the start of a lava-dome eruption on October 16, 1980—the first lava-dome eruption of the 1980s to produce a dome that survived. The last lava-dome eruption of the 1980s was on October 21, 1986, and the last significant SO_2 emission rate at the end of this eruption was 80 t/d on December 9, 1986. Of the 113 SO_2 emission-rate measurements made after this date, until measurements ceased on September 6, 1988, 95 percent were <25 t/d and 70 percent were <3 t/d—barely above detection limits. We did not include these data in the MWRST analysis in order to avoid confounding the emission rates associated with the 1980s lava-dome eruptions with emission rates of the protracted period of residual degassing at the end of the 1980s eruption cycle. The1980s dataset for the calculations started with the data from December 9, 1986, and was extended back in time by incrementally adding earlier SO_2 emission rates. Along this time line, the probability level decreased steadily from P >0.05 and converged on the critical significance level (P = 0.05) when the October 18, 1980, data were added to the dataset. When still earlier 1980 data were included, P dropped abruptly below 0.05, indicating that the difference between the two groups of data became robustly significant. Thus, between October 18, 1980, and December 9, 1986, the two groups of data sample a similar population, and the differences between them—for example, median SO_2 emission rates of 72 t/d versus 100 t/d—can be explained by random sampling variations. However, we stress that the MWRST analysis operates only on the rates of the two groups of data without regard for the associated dates. This is important because if the dates are considered, it is evident that although the 10/18/1980–12/9/1986 SO_2 emission rates may share a common population with 2004–5 SO_2 emission rates, they are not randomly distributed in time, as indicated by the conspicuous skewing of their higher rates to earlier dates (fig. 16).

Plotting the SO_2 emission rates of the 1980s and 2004–5 together as time series on the same scale reveals that the emission rates of the 2004–5 eruption appear similar to those of the 1980s lava-dome eruptions back to at least late 1981 (fig. 16). MWRST comparisons back to late 1981 produce large P values indicating virtually no likelihood of a significant difference in the SO_2 emission rates of the 1980s and 2004–5 lava-dome eruptions; for example, comparisons back to October 1, 1981, give a P value of 0.7. Such differences as exist in the patterns of the two time-series plots are readily explained. The generally lower peak values of the 2004–5 eruption probably are related to the more-crystalline magma and steadier character of the present eruption; these properties act to curb extrusive surges that frequently caused SO_2 emission-rate peaks during the 1980s lava-dome eruptions. The 2004–5 emission rates appear blockier and less spiky on the graph, partly because of the steadier nature of the present eruption, but also because the steadier activity itself (along with tighter funding) led to less frequent monitoring flights—four to five times less frequent than in the 1980s. The fact that the current eruption has lasted considerably longer than the 1980s lava-dome eruptions also contributes to the blockier pattern of its SO_2 emission rates. The annualized 2004–5 SO_2 outputs also bear a noteworthy similarity to annual SO_2 outputs that occurred during the later years of the 1980s lava-dome eruptions. The 14-month, 30,000-t SO_2 output of the 2004–5 eruption (table 2) indicates an annualized output of 26,000 t, which is equivalent to the total Mount St. Helens SO_2 output for 1984 (Gerlach and McGee, 1994)—a year in which there were three lava-dome eruptions over a 6-month period. The 11-month output for 2005 of 18,000 t (computed from table 2 data) annualizes to an output of 19,600 t—comparable with the 1986 SO_2 output of 17,000 t (Gerlach and McGee, 1994). Thus, the MWRST analyses, the time-series patterns of SO_2 emission rates, and the annualized SO_2 outputs strongly suggest that the 2004–5 SO_2 emissions are similar to those of the 1980s lava-dome eruptions, possibly back as far as late 1981 or late 1980.

The CO_2 emission-rate measurements of the 1980s are restricted to the period between July 1980 and August 1981 (fig. 17; McGee and Casadevall, 1994); the measurements were terminated after August 1981 because the detection limit of the older measurement technique was reached. Applications of the MWRST to these data and the 2004–5 CO_2 emission-rate data (fig. 7, table 2), following the procedure described

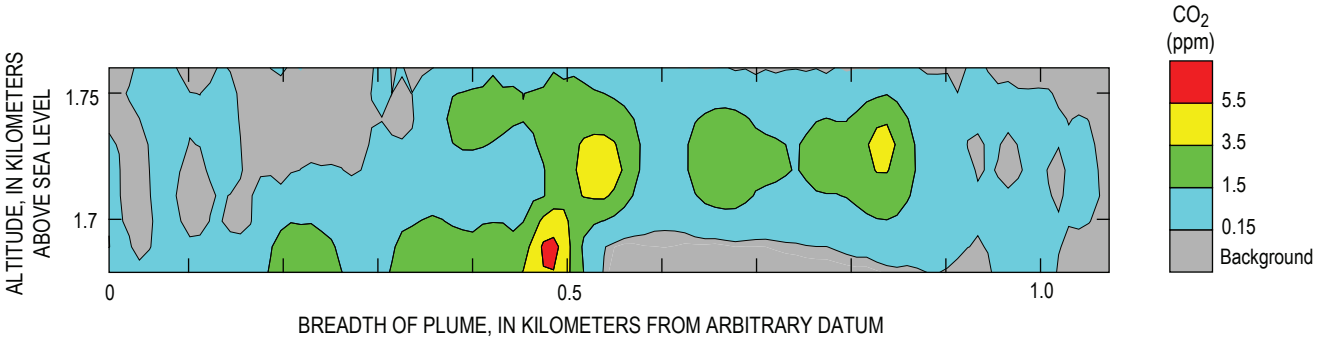

Figure 15. Vertical cross section of CO_2 gas plume 250 m downwind of Loowit springs area on June 9, 2005. The CO_2 emission rate computed from these data was 27 t/d. Scale bar on right shows CO_2 concentration above local atmospheric background.

above for comparing SO_2 emission rates, indicates that the 2004–5 data are significantly different from the July 1980–May 1981 data ($P \leq 0.05$). However, the 2004–5 data and the June–August 1981 data are not different and appear to be sampling the same population ($P > 0.05$). The similarity probably would have persisted beyond August 1981 had measurements been made by a more sensitive technique. Plotting the CO_2 emission rates of 1980–81 and 2004–5 together as time series on the same scale reinforces the MWRST analysis by revealing a pattern in which the latter CO_2 emission rates appear as an extension of the lower CO_2 emission rates of June–August 1981 (fig. 17). As in the case of the SO_2 emission rates, differences in magma physical properties and frequency of measurement account for the blockier, less spiky, and generally lower peak values of the 2004–5 CO_2 emission rates.

Thus, the time-series comparisons and MWRST results for CO_2 and SO_2 emission rates support a flat 2004–5 magma depleted in excess volatiles and producing generally low CO_2 and SO_2 emissions like those of the 1980s lava-dome eruptions. The flat magma is distinctly different from the gas-rich magma that produced the much higher CO_2 and SO_2 emissions earlier in 1980 (figs. 16, 17; Gerlach and McGee, 1994). The similarity to the gas emissions of the 1980s lava-dome eruptions suggests that the flat magma of the current eruption could involve leftover reservoir magma from 1986.

Comparison with 1980s CO_2/SO_2 Ratios

Contemporaneous measurements of CO_2 and SO_2 emission rates in the 1980s allow calculation of CO_2/SO_2 ratios on 117 days during a 418-day period from July 6, 1980, to August 28, 1981. The median CO_2/SO_2 ratio is 8, but there is considerable variation—25 percent of the ratios are ≤5 and 25 percent are ≥11. As noted earlier, measured and weighted CO_2 and SO_2 emission rates and total emissions of the current eruption imply a somewhat higher grand median CO_2/SO_2 ratio of 11±1. The MWRST indicates that the 117 1980–1981 CO_2/SO_2 ratios and the 24 2004–5 CO_2/SO_2 ratios—whether calculated from measured or weighted emission rates—are associated with significantly different populations ($P < 0.05$). Taking these results at face value would imply a real difference in CO_2/SO_2 ratios of the older and current gases, but we show below that the higher CO_2/SO_2 ratios of the current gases are caused by scrubbing.

Scrubbing in the 2004–2005 Eruption

Doukas and Gerlach (1995) drew attention to the unusually weak SO_2 emission rates that both preceded and followed eruptions at Crater Peak on Mount Spurr volcano, Alaska, in 1992 and noted the exceptionally strong and persistent H_2S odor in the Crater Peak plume during repose periods. They argued that liquid water present at or beneath the surface interacted with ascending magmatic gases, scrubbing SO_2 and other strongly acidic gases (HCl, HF) but impacting the weakly and moderately acidic gases (CO_2 and H_2S) less severely. The principal mechanisms for SO_2 scrubbing by liquid water are the hydrolysis reactions:

$$4SO_{2(g)} + 4H_2O_{(l)} = H_2S_{(g)} + 6H^+_{(aq)} + 3SO_4^{-2}{}_{(aq)}, \text{ and}$$

$$3SO_{2(g)} + 2H_2O_{(l)} = S_{(l,s)} + 4H^+_{(aq)} + 2SO_4^{-2}{}_{(aq)}.$$

These equilibria shift strongly to the right below 400°C, mainly converting SO_2 into dissolved sulfate as sulfuric acid. Some H_2S gas and native sulfur also are generated, which explained the intense H_2S odor at Crater Peak. Detailed thermochemical modeling (Symonds and others, 2001) confirms the significant scrubbing of magmatic SO_2, HCl, and HF by contact with surface, ground, and hydrothermal waters of volcanoes and indicates that scrubbing of CO_2 and H_2S also becomes significant at low gas-to-water ratios (<0.01, mass basis).

Carbon isotopes of dissolved inorganic carbon in hydrothermal, ground, spring, and stream waters reveal the scrubbing of magmatic CO_2 in the vicinity of several Cascade Range volcanoes: Lassen Peak, Mount Shasta, Crater Lake, Mount Bachelor, Broken Top, Three Sisters, Belknap Crater, and Mount Jefferson (Rose and Davisson, 1996; James and others, 1999; Evans and others, 2004). Scrubbing of potentially coexisting, more acidic magmatic gases (SO_2, H_2S, HCl, and HF) also probably occurs. Copious ground-water recharge in the High Cascades and subsequent downward and lateral flow (Ingebritsen and others, 1989, 1992, 1994) is probably chiefly responsible for the scrubbing and provides a basis for a conceptual model of scrubbing throughout much of the Cascade Range. Scrubbing processes may, therefore, be responsible for the currently absent to negligible emission rates of CO_2, SO_2, and H_2S at several Cascade Range volcanoes we have investigated with airborne measurements since the late 1990s (table 1). Although some of these volcanoes (for example, Mount Adams and Mount Jefferson) may simply be dormant, it is likely that much of the CO_2, SO_2, H_2S, HCl, and HF degassed from magmas at most of these volcanoes is captured by hydrothermal systems or ground water and is thus unavailable to form gas emissions at volcanic centers. Boiling of hydrothermal fluid containing captured magmatic gases may give rise to persistent degassing of CO_2 and H_2S (but not SO_2 because of hydrolysis to dissolved sulfate) at some volcanoes—Mount Baker and Lassen Peak being likely examples (table 1).

Symonds and others (2001) applied their thermochemical scrubbing models to several eruptions, including the 1980 eruption of Mount St. Helens, which they say illustrates SO_2 scrubbing in the early stage of an eruption. Low SO_2 emission rates—from less than 10 t/d to 48 t/d—during the period of phreatic eruptions and nonexplosive degassing that began on March 27, 1980, continued for 52 days up to the May 18 climactic explosion. Observations supporting early scrubbing of SO_2 include reports by COSPEC investigators of persistent H_2S odor in the crater at times when SO_2 emissions rarely exceeded 10 t/d (Stoiber and others, 1980). Emission rates of

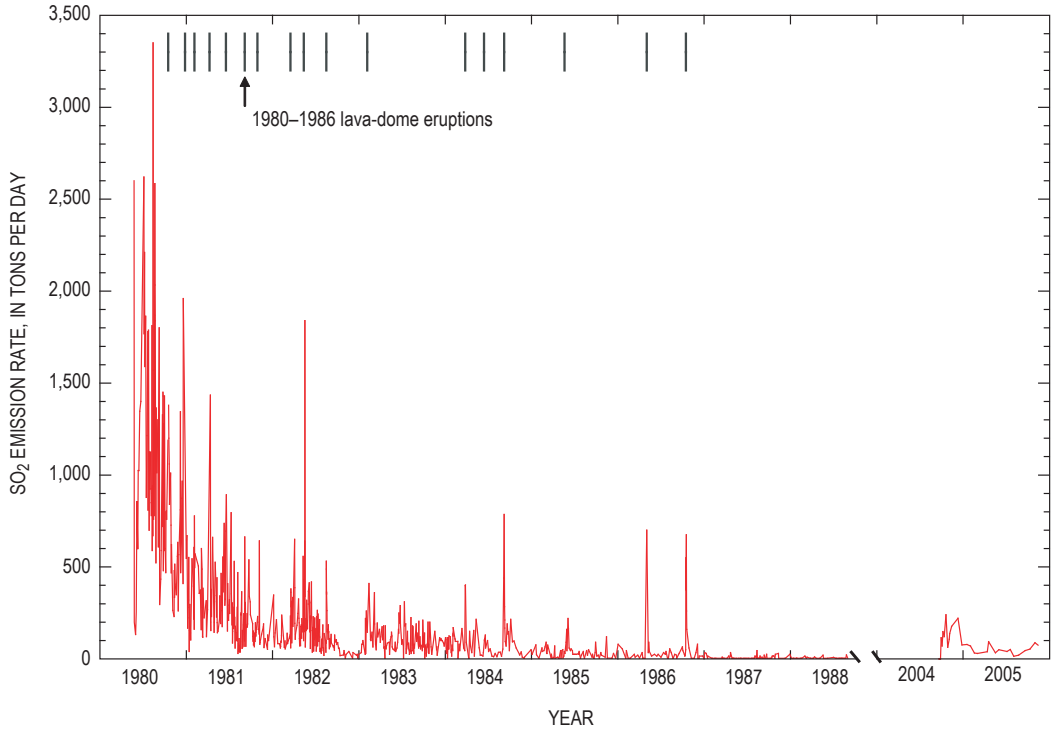

Figure 16. Time-series plots of all SO_2 emission rates measured during the 1980s (McGee and Casadevall, 1994) and during the 2004–2005 eruption. Scale break after last 1980s measurements in 1988 separates the two time series. Vertical lines indicate the starting dates of the 1980–1986 lava-dome eruptions. All 1980s and 2004–2005 time-series data are passive emission rates, except for the first 1980 data point—2,600 t/d measured in the May 25, 1980, explosive eruption. The May 18, 1980, explosive emission rate of 4,000,000 t/d is not included (Gerlach and McGee, 1994; Symonds and others, 2001).

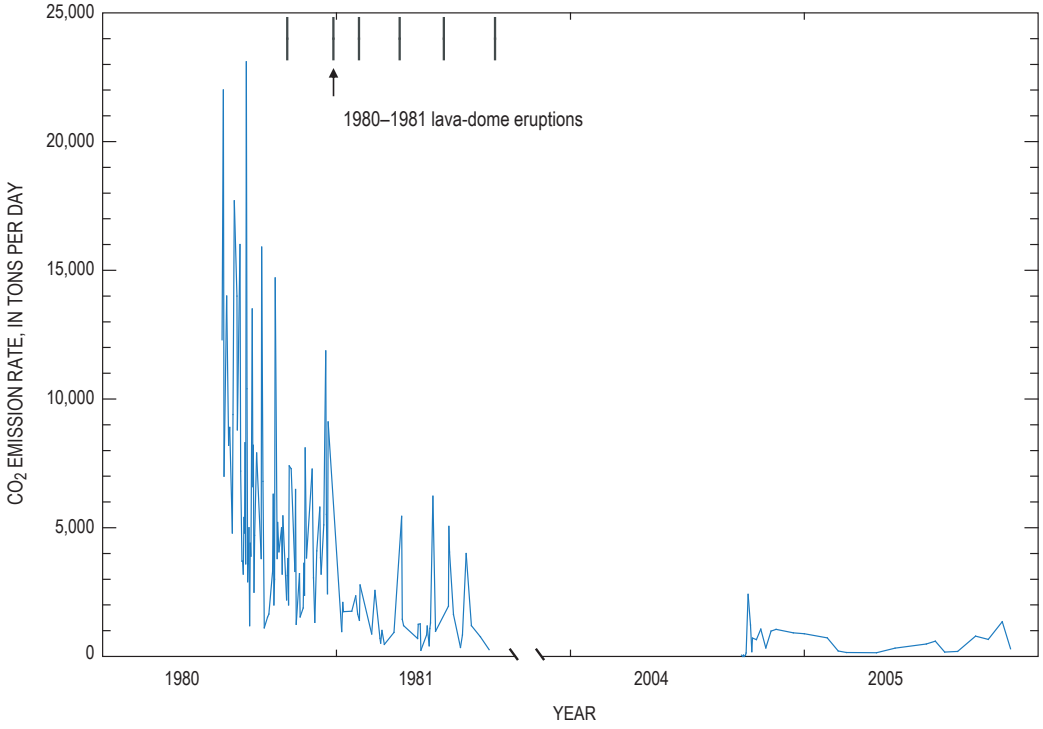

Figure 17. Time-series plots of all CO_2 emission rates measured during the 1980s (McGee and Casadevall, 1994) and during the 2004–2005 eruption. Scale break after the last measurements in 1981 separates the two time series. Vertical lines indicate starting dates of the 1980–1981 lava-dome eruptions. All 1980s and 2004–2005 time-series data are passive emission rates. The 1980 data begin with the 12,300 t/d CO_2 emission rate measured on July 6.

passively degassed SO_2 increased after the May 18 eruption and after the second explosion on May 25 but still remained relatively low (130–260 t/d). Twenty days later, on June 6, SO_2 emission rates jumped to 860 t/d and remained high (>600 t/d) until the end of October 1980 (fig. 16), finally attaining levels comparable to those of other erupting arc volcanoes and signaling the end of significant scrubbing. Note that the July 6, 1980, to August 28, 1981, CO_2/SO_2 ratios discussed above represent postscrubbing values.

Symonds and others (2001) also inferred that SO_2 scrubbing was active again during the period of seismic unrest at Mount St. Helens in the summer of 1998 when, as described above, an airborne survey on June 22 measured a CO_2 emission rate of 1,900 t/d (table 1), while concurrent COSPEC measurements failed to detect SO_2. These results are consistent with the degassing and scrubbing of SO_2 from an intrusion at a time when melting of snow from a permanent snowfield growing in the crater since 1986 (Anderson and others, 1998) helped create a wet edifice. Thus, an unknown amount of degassed CO_2 may also have been scrubbed at this time.

Scrubbing played a major role in the period of unrest and the early stages of the current eruption. We interpret the measurements during the September 27–30, 2004, period of insignificant gas emission with little or no detectable SO_2 or H_2S and with CO_2 largely at atmospheric levels (fig. 9) to be the result of fairly complete gas scrubbing at low gas-to-water mass ratios <0.01 (Symonds and others, 2001). Sealing of rock permeability in the old dome and the upper part of the 1980s conduit may also have played a role (Moran, 1994). It is likely, however, that scrubbing would soon have dominated sealing as a deterrent to gas emission. The concurrent shallow seismicity and deformation would tend to reestablish permeability. High seismicity was well established by September 26 and increased significantly on September 28 at shallow levels in and below the old lava dome (Moran and others, this volume, chap. 2). Radial fractures were visible in Crater Glacier adjacent to the old dome by September 26, and an area of deformation south of the dome was clearly evident on oblique photos on September 30 (Schilling and others, this volume, chap. 8). Furthermore, the 2004 unrest and eruption followed a period with an unusually large potential for ground-water recharge by surface water. No August–September interval since the cessation of dome-building eruptions in 1986 has had heavier rainfall than in 2004 (http://www.wcc.nrcs.usda.gov/snotel, last accessed March 15, 2008). The growth of Crater Glacier since 1986 provided increased storage of water available for release and ground-water recharge into late summer. Moreover, the earlier detection of sharp CO_2 concentration spikes on October 1 and 2, while SO_2 and H_2S remained at detection limits (fig. 10), strongly suggests scrubbing, rather than sealing, as the main cause restricting earlier gas emissions, since water does not scrub CO_2 as effectively as it scrubs SO_2 and H_2S. The subsequent appearance of wet degassing with large gas bubbles ejecting through pools of water obviously involved scrubbing. However, the subequal concentrations of SO_2 and H_2S at this time (fig. 11) reflected incomplete scrubbing of SO_2, which is likely because rapid transport in large bubbles restricted its interaction with water, thus allowing some of it to escape the pools. Wet degassing increasingly gave way to dry degassing, and SO_2 became the major sulfur gas (fig. 12). As temperatures rose and steaming increased, rock adjacent to the invading magma progressively dried out in the days before the initial emergence of a lava spine from the deforming area south of the 1980s dome on October 11. This date probably marks the end of significant scrubbing in the early stages of the eruption.

The composite degassing sources from the 1980s and 2004–5 domes bear the mark of gas scrubbing (fig. 14). Nearly all of the SO_2 in the plume comes from the hotter new dome. Degassing from the colder old dome involves minor CO_2 but little or no SO_2. We speculate that the source of gas at depth is the same for both domes but that the gas feeding the vents on the old dome is scrubbed of its SO_2 since water is more likely to be present within and beneath this colder dome. Edmonds and others (this volume, chap. 27) measured several gases, including SO_2 and HCl, in hot vent emissions on the new dome by remote Fourier-transform infrared spectroscopy from high on the east rim of Mount St. Helens. If our hypothesis is correct, both SO_2 and HCl—being strong acids—should be scrubbed in emissions from the old dome. Unfortunately, confirmation of concurrent scrubbing of both SO_2 and HCl at the old dome by similar measurements was not possible, owing to the absence of hot infrared sources.

The 24 CO_2/SO_2 ratios calculated from cumulative CO_2 and SO_2 emissions (fig. 8; table 2) show a striking pattern when plotted as a time series (fig. 18). The ratios decrease regularly and precipitously from October 7 until October 27, 2004, when they make a abrupt transition to nearly constant CO_2/SO_2 values of 9±1, close to the median value of 8 noted above for the 1980–81 CO_2/SO_2. They remain in this range (9±1) until September 28, 2005, after which subsequent 2005 values drift to CO_2/SO_2 values as high as 11.3.

We interpret the sharp decline in CO_2/SO_2 (fig. 18) to reflect the drying out of the shallow conduit and crater-floor rock adjacent to the invading dacite and the reduction of SO_2 scrubbing that dominated the early part of the 2004–5 eruption. However, cumulative emissions, although smoothing out short-term variations, can lag in their response to significant changes. In this case, measurements suggest early SO_2 scrubbing largely ceased on or about October 11, 2004, as discussed above, approximately two weeks before the October 27 date suggested by the cumulative emission data (fig. 18). After October 27, the CO_2/SO_2 ratio of cumulative emissions stabilized within the range of 9±1 for many months, grazing the median 1980–81 CO_2/SO_2 value of 8 (fig. 18). We interpret this range of values to represent the CO_2/SO_2 of nonscrubbed gas emissions of the current eruption, although it may be slightly high because of SO_2 scrubbing of gases from the old dome. The CO_2/SO_2 of the cumulative emissions rises above this range again after September 28, 2005 (fig. 18), presumably in response to renewed scrubbing. Because of the lag effect, the return to scrubbing may have started somewhat earlier. We have no data suggesting

a specific cause of this return to scrubbing, but plausible factors may include the cracking and development of fracture permeability within the cooling and thickening carapace of the new dome and (or) seasonal changes affecting rainfall and groundwater recharge in the crater.

The CO_2/SO_2 time-series pattern in figure 18 illustrates the role of scrubbing in the early part of the current eruption and the close similarity of CO_2/SO_2 values in the nonscrubbed gas emissions of the 2004–5 eruption to those in the early 1980s. We contend, moreover, that scrubbing is the cause of the significant difference in CO_2/SO_2 indicated between the 1980–81 and 2004–5 gases by the MWRST analysis. The striking pattern of CO_2/SO_2 ratios (fig. 18) with their approach to the median 1980–81 CO_2/SO_2 ratio, hardly seems the result of chance, and it is consistent with flat magma remaining from 1986 that, although depleted in excess volatiles, still retains a similar CO_2/SO_2 ratio. However, the depletion of excess volatiles causes the emissions from the flat magma upon ascent and eruption to be generally weak and susceptible to scrubbing if water is present.

Fluid Content of the 2004–2005 Dacite at Depth

Recent studies indicate that the dacite erupted explosively at Mount St. Helens on May 18, 1980, had a fluid content (that is, excess volatiles) prior to ascent and eruption of ≥15 volume percent (vol. percent), which corresponds to ≥3 weight percent (wt. percent) (Wallace, 2001, 2003; P.J. Wallace, written commun., 2005). The May 18, 1980, dacite was decidedly not flat magma. We have tested the flat-magma hypothesis for the 2004–5 dacite by using the current CO_2 emission data to quantify the fluid content of the 2004–5 dacite at depth. If the flat-magma hypothesis is valid for the current dacite, its fluid content at depth should be significantly lower than that determined for the May 18, 1980, dacite.

Fluid Content of the 2004–2005 Dacite and the May 18, 1980, Dacite at 900°C and 220 MPa (8.6 km Depth)

The May 18, 1980, dacite last equilibrated prior to eruption at a temperature of 900°C and a pressure of 220 MPa (Rutherford, 1993), corresponding to 8.6 km depth (from crustal density model B-B' of Williams and others, 1987, used in this study to convert lithostatic pressures to depths beneath the crater). The rhyolitic melt of the May 18 dacite was relatively H_2O rich prior to eruption. Microprobe studies of melt inclusions give water-by-difference concentrations of 4.6±1 wt. percent (Rutherford, 1993), and recent ion-microprobe studies of melt inclusions in the May 18 white pumice show a clustering of H_2O concentrations around 5 wt. percent (Blundy and Cashman, 2005).

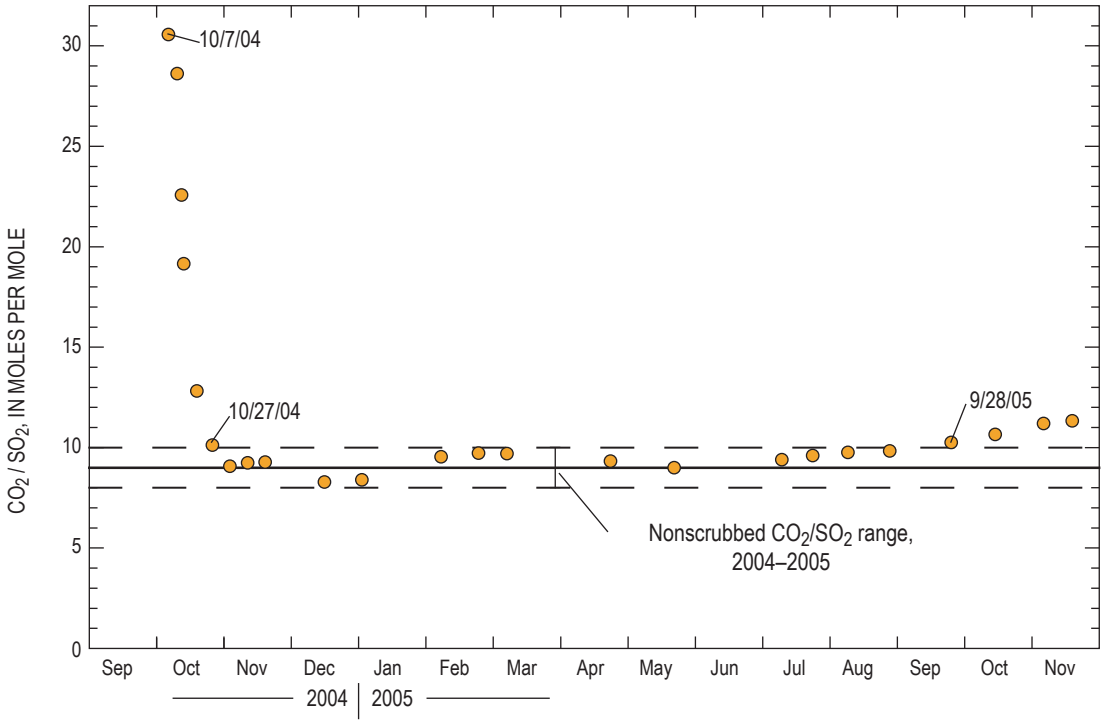

Figure 18. Time-series plot of molar CO_2/SO_2 ratios (dots) calculated from cumulative 2004–2005 emissions (fig. 8; table 2). Solid and dashed lines indicate nonscrubbed CO_2/SO_2 median and range of 9±1 for the 2004–5 gases. Lower dashed line also represents the median value (8) of the 1980–81 CO_2/SO_2 ratios as discussed in the text.

To maintain comparability with the May 18 dacite, we have used the constraints 900°C, 220 MPa, and a rhyolitic melt H_2O concentration of 5 wt. percent to estimate the fluid content of the 2004–5 dacite at 8.6 km depth. Several observations and experimental results support the use of these constraints. The current dacite contains phenocrysts of plagioclase, hypersthene, amphibole, and oxides—the same as the 1980–86 dacite, except for an absence of minor clinopyroxene (Pallister and others, this volume, chap. 30; Rutherford and Devine, this volume, chap. 31). The current dacite also is similar in bulk composition to the 1980–86 dacite, being only slightly more evolved (65 vs. 63 wt. percent SiO_2) and distinct in U-series isotopic ratios of plagioclases (Cooper and Donnelly, this volume, chap. 36) and in bulk-composition ratios of Ti and Cr to SiO_2 (Pallister and others, this volume, chap. 30)—differences that are most readily explained by addition of a minor fraction of new magma to the reservoir between 1986 and 2004 (Pallister and others, this volume, chap. 30). Melt inclusions provide no data on the H_2O concentration of preeruption melt in the current dacite (Pallister and others, this volume, chap. 30; Rutherford and Devine, this volume, chap. 31; Blundy and others, this volume, chap. 33). However, on the basis of phase equilibria experiments, Rutherford and Devine (this volume, chap. 31) propose that the new magma entered the storage reservoir as dacite with a melt concentration >4 wt. percent—implied by the amphiboles—and at a temperature of ~900°C—suggested by high-TiO_2 magnetite phenocrysts and the maximum anorthite content of cyclically zoned feldspar phenocrysts. These conditions are similar to those determined for the 1980 magma. To explain the cyclic zoning of the magma's phenocrysts, Rutherford and Devine invoke convective circulation of injected dacite, which would have involved exposure to pressures of 220 MPa at various times before rising to the shallower part of the reservoir, where they infer it last equilibrated at about 850°C and 120–140 MPa prior to final ascent and eruption.

We used VolatileCalc (Newman and H_2O Lowenstern, 2002) to model CO_2 solubility in hydrous rhyolitic melt at 900°C and 220 MPa to estimate the fluid content of the 2004–5 dacite for comparison with the May 18 dacite at 8.6 km depth. At these conditions, rhyolitic melt with 5 wt. percent H_2O would contain associated dissolved CO_2 at a concentration of ~350 ppm (fig. 19*A*). The mole fraction composition of the coexisting fluid would be ~0.76 for X_{H_2O} and ~0.24 for X_{CO_2} (fig. 19*B*), which is consistent with hydrothermal phase equilibria experiments on the current dacite that indicate X_{H_2O} would be ≥0.7 in the presence of a CO_2-bearing coexisting fluid (Rutherford and Devine, this volume, chap. 31). The fluid also would contain a small amount of sulfur, but since CO_2/SO_2 is ~9 in the nonscrubbed gas emissions—and CO_2/S would likely have been higher in the fluid at elevated pressure—we ignore sulfur in the present analysis.

We calculated the fluid content of the dacite at 8.6 km and the conditions delineated above for 14 dates in 2004–5 corresponding to the dates of digital elevation models (DEMs; Schilling and others, this volume, chap. 8). Table 3 lists values keyed to DEM dates for several parameters (defined in table 3 headnotes) used in the calculations. The last 2005 DEM date (12/15/2005) could not be used because weather conditions prevented measurement of CO_2 emission rates during December 2005, as noted above.

Table 3 contains values for two melt mass parameters: one for dacite like the 2004–5 dacite that contained 53.5 vol. percent melt prior to eruption (Pallister and others, this volume, chap. 30), which we discuss later, and the other for preeruption dacite with 70 vol. percent melt. The 70-vol. percent case for melt masses is based on the groundmass abundances of 65–80 vol. percent reported for the somewhat less evolved May 18, 1980, white pumice (Cashman and Taggert, 1983; Rutherford and others, 1985; Cashman, 1992) and a

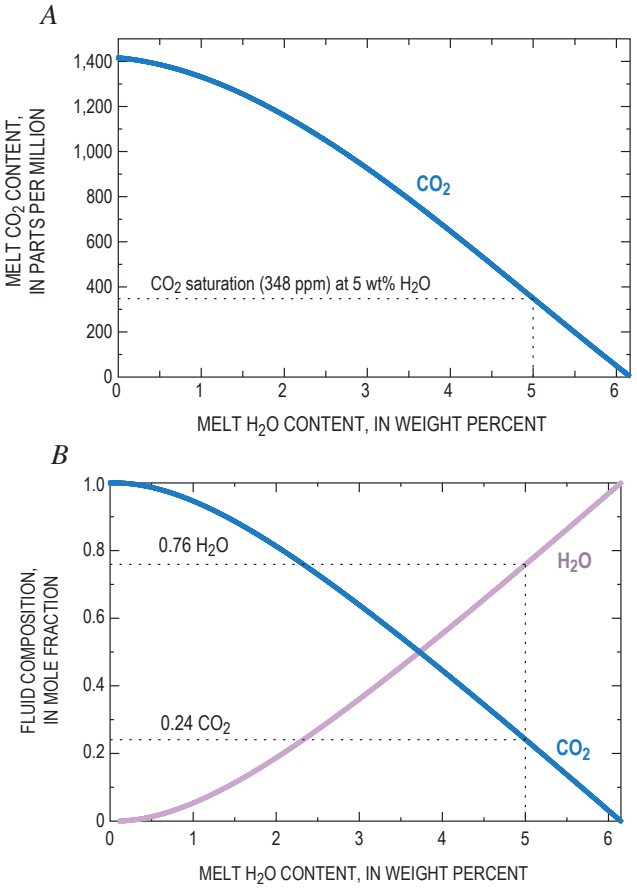

Figure 19. Concentration of CO_2 in hydrous rhyolitic melt and coexisting fluid composition at 220 MPa and 900°C (Newman and Lowenstern, 2002). *A*, Solubility of CO_2 (solid blue curve) in hydrous rhyolitic melts with a range of water concentrations. Dotted lines indicate a CO_2 saturation limit of 348 ppm for rhyolitic melt containing 5 wt. percent H_2O. Melt H_2O content is total H_2O—that is, OH and molecular H_2O. *B*, Mole fraction concentrations of H_2O and CO_2 (solid curves) in fluids coexisting with hydrous rhyolitic melts over a range of water concentrations. Dotted lines indicate fluid composition of 0.76 X_{H_2O} and 0.24 X_{CO_2} coexisting with rhyolitic melt containing 5 wt. percent water.

Table 3. Parameters for calculation of fluid content of the 2004–2005 dacite, Mount St. Helens, Washington.

[Digital elevation model (DEM) dates are the dates of DEMs of Schilling and others (this volume, chap. 8). Dacite volumes are estimated cumulative volumes of the newly extruded lava dome (Schilling and others, this volume, chap. 8). Dense rock equivalent (DRE) volumes are cumulative dacite volumes adjusted for an average porosity of 10 vol. percent (Cashman and others, this volume, chap. 19; Pallister and others, this volume, chap. 30; C. Thornber, written commun., 2006). Dacite masses are cumulative masses in metric tons (t) of dacite derived from the DRE volumes and the dacite DRE density of 2.62 g/cm^3 (K. Russell, written commun., 2006). Melt masses (t) are cumulative masses of melt estimated from DRE volumes and preeruption melt fractions of 53.5 vol. percent and 70 vol. percent, as described in the text. CO_2 masses (t) are cumulative masses of CO_2 output as of each DEM date, calculated from a curve fit to the cumulative CO_2 emissions (fig. 8). Significant figures were exaggerated to reduce roundoff errors.]

DEM date	Dacite volume (10^6 m^3)	DRE volume (10^6 m^3)	Dacite mass (10^6 t)	Melt mass for 53.5 vol. percent melt (10^6 t)	Melt mass for 70 vol. percent melt (10^6 t)	CO_2 mass (t)
11/04/2004	11.8	10.62	27.82	13.07	17.10	23,482
11/20/2004	18.4	16.56	43.39	20.38	26.66	39,380
11/29/2004	21.3	19.17	50.23	23.59	30.86	48,800
12/11/2004	25.5	22.95	60.13	28.24	36.95	61,162
01/03/2005	30.5	27.45	71.92	33.78	44.19	82,459
02/01/2005	35.1	31.59	82.77	38.87	50.86	102,639
02/21/2005	39.2	35.28	92.43	43.41	56.80	112,188
03/10/2005	41.9	37.71	98.80	46.40	60.71	118,092
04/19/2005	47.5	42.75	112.01	52.60	68.83	127,630
06/15/2005	53.9	48.51	127.10	59.69	78.10	141,901
07/14/2005	57.1	51.39	134.64	63.24	82.74	152,123
08/10/2005	61.7	55.53	145.49	68.33	89.40	163,184
09/20/2005	67.3	60.57	158.69	74.53	97.52	182,139
10/24/2005	70.0	63.00	165.06	77.52	101.43	202,885

melt density of 2.3 g/cm^3 reported for experimental investigations of rhyolite densities at elevated temperature and water pressure (Silver and others, 1990). The 70-vol. percent case maintains comparability with 1980 conditions of 900°C, 220 MPa, and rhyolitic melt containing 5 wt. percent dissolved H_2O at 8.6 km depth.

For each DEM date, the amount of dissolved CO_2 was calculated from the concentration of CO_2 in the melt (fig. 19*A*) and the mass of melt for the DEM date (table 3), as estimated from the 70-vol. percent melt fraction discussed above. In all cases, the amount of dissolved CO_2 was a minor fraction (<20 percent) of the cumulative (total) CO_2 output as of the DEM date (table 3), indicating that 2004–5 dacite containing 70 vol. percent rhyolitic melt with 5 wt. percent dissolved H_2O would indeed have been fluid saturated in the magma reservoir at 900°C and 220 MPa (8.6 km depth). We determined the amount of CO_2 in the fluid phase by subtracting the amount of CO_2 dissolved in the melt from the cumulative CO_2 emitted as of the DEM date (table 3). Having determined the amount of fluid CO_2, we calculated the amount of fluid H_2O from the H_2O-CO_2 fluid compositional relation (fig. 19*B*). We converted the amounts of fluid CO_2 and H_2O into a fluid volume by assuming ideal mixing and by using the modified Redlich-Kwong (MRK) equation of state (Holloway, 1977, 1981) to calculate molar volumes of CO_2 and H_2O at 900°C and 220 MPa. The volume of fluid and the DEM-based dacite volume (table 3), corrected to dense rock equivalent (DRE) basis (table 3), gave the fluid content as a volume percent of the dacite. The dacite masses (table 3) and the amounts of fluid CO_2 and H_2O also allowed expression of the fluid content as a weight percent of the dacite.

Figure 20 shows the fluid content of the dacite for the 14 DEM dates at 900°C and 220 MPa (8.6 km depth). The results, ranging from 0.82 to 1.32 vol. percent (0.15–0.24 wt. percent), indicate steady fluid content for the dacite at 8.6 km depth after a brief period of regularly increasing values involving the points for the first four DEM dates (November–December 2004). Steady fluid content begins with the January 3, 2005, DEM date and continues thereafter; it ranges from 1.16 to 1.32 vol. percent (0.21–0.24 wt. percent) and averages 1.23 vol. percent (0.22 wt. percent). These results are consistent with those of Mastin and others (this volume, chap. 22), who also inferred a low reservoir fluid content of <1.5 vol. percent from the relation between erupted-dacite volume and the volume shrinkage of the reservoir obtained from geodetic data (Lisowski and others, this volume, chap. 15).

It is noteworthy that the results are steady throughout 2005 despite the disparate datasets involved. Several factors may be at work during the brief period involving the four points of lower but steadily rising fluid content during November–December 2004 (fig. 20). These factors probably reflect the declining influence with time of CO_2 lost in scrubbing prior to November 2004 (or missed if airborne measurements were too infrequent) on the cumulative CO_2 output. Increasing the cumulative CO_2 outputs by 38 percent (11/4/2004) to 15 percent (12/11/2004) would bring the four points into the steady range of values. Alternatively, the lower fluid content may reflect a higher porosity of the earlier dacite—somewhere in the range 11–32 vol. percent (K. Russell, written commun., 2006)—compared to the eruption average of 10 vol. percent (table 3) used in the calculations, although there is presently no evidence that porosity declined in a steady way early in the eruption. A higher porosity decreases the DRE volume and mass of dacite in proportion to the cumulative amount of CO_2 and causes the volume percent fluid for the four 2004 DEM dates to increase—porosities of 35 vol. percent (11/4/2004) to 22 vol. percent (12/11/2004) would cause the fluid content of these dates to fall within the range of steady 2005 results. Involvement of shallower, more degassed magma early in the eruption might also account for the lower 2004 fluid content, but it is not obvious from the CO_2 emissions that the earlier magma was more degassed (figs. 7, 17). Lastly, the procedures used to estimate dacite volumes from DEMs may overestimate the smaller dacite volumes of the eruption-startup period, causing erroneously low calculated fluid content. Significant underestimation of early dacite volumes seems more likely, however, because of unaccounted for dacite residing in the conduit. Apparently, the volume of conduit dacite became a negligible fraction of the measurable dacite volume fairly early—sometime prior to the first DEM on 11/4/2004 (table 3).

The sensitivity of the modeling to the volume percent melt-fraction parameter is an important concern that is easily addressed. Recalculating the model for a melt fraction of 53.5 vol. percent (table 3), compared to the 70-vol. percent melt fraction used above, illustrates the low sensitivity of the results to a plausible range of values for the volume percent melt parameter. The resulting steady 2005 fluid content ranges from 1.23 to 1.39 vol. percent and averages 1.29 vol. percent—hardly different from the above results for 70 vol. percent melt.

Recently, Liu and others (2005) derived a new empirical model of CO_2 and H_2O solubility in fluid-saturated rhyolitic melt and recommended it over VolatileCalc (Newman and Lowenstern, 2002) for eruptive degassing and magma-chamber dynamics calculations because it gives better fits to experimental solubility data, especially at pressures above 200 MPa. At the conditions considered here, though, the two models agree closely on the dacite fluid content. For example, during the period of steady 2005 DEM dates, the model of Liu and others (2005) gives 1.17–1.33 vol. percent and a 1.24-vol. percent average versus 1.16–1.32 vol. percent and a 1.23-vol. percent average by VolatileCalc. The agreement becomes virtually exact in calculations at the lower pressures considered below. For these reasons, and because of VolatileCalc's user-friendly software, we have used it throughout this study.

We conclude that the average steady 2005 fluid content of 1.23 vol. percent (0.22 wt. percent; fig. 20) is the best estimate of the fluid content of the current dacite at a reservoir depth of 8.6 km, 900°C, and 220 MPa. This result and, indeed, all the results obtained above are significantly less than the ≥15-vol. percent (≥3 wt. percent) fluid determined for the May 18 dac-

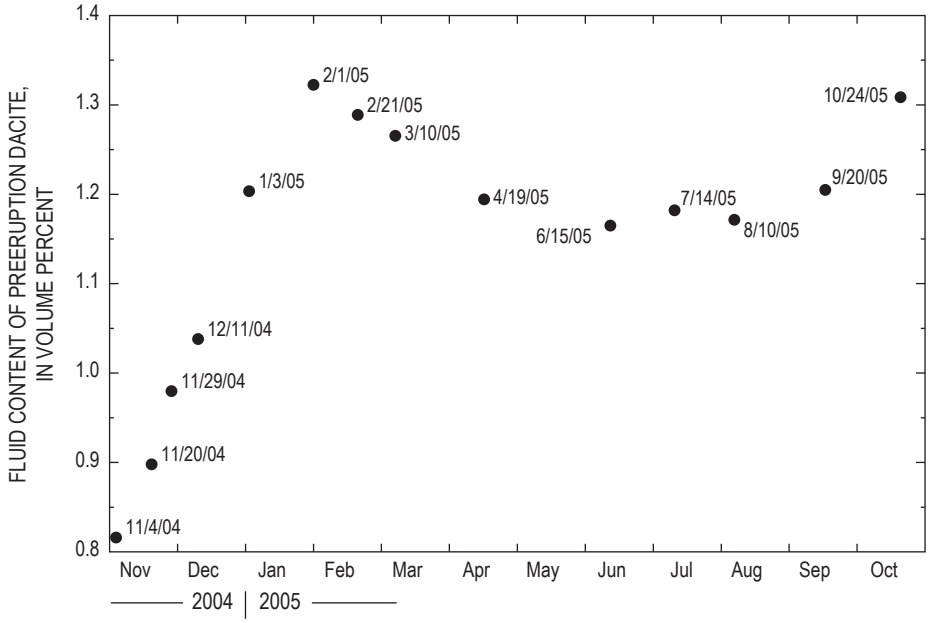

Figure 20. Fluid content of dacite at 900°C and 220 MPa (8.6 km) calculated as described in the text for 14 DEM dates in 2004–5.

ite; furthermore, they are much less than the 5–30-vol. percent (1–6 wt. percent) fluid indicated for several other explosive eruptions of silicic and intermediate magma (Wallace, 2001, 2003). The present analysis, therefore, indicates depletion of excess volatiles and thus confirms the flat-magma hypothesis for the dacite of the 2004–5 eruption.

Fluid Content of the 2004–2005 Dacite Prior to Ascent at 850°C and 130 MPa (5.2 km Depth)

As the dacite migrates to reservoir depths shallower than 8.6 km, its fluid content increases. Of particular interest is the fluid content where the dacite last equilibrated at about 850°C and 120–140 MPa in the presence of an H_2O-rich fluid ($X_{H_2O} \approx 1$) prior to ascent and eruption (Rutherford and Devine, this volume, chap. 31). The corresponding depth range of 4.8–5.6 km (Williams and others, 1987) places the preeruption dacite in the shallowest part of the ellipsoidal-cylindrical magma reservoir extending from 4.5–5 km to ≥12 km, as indicated by deformation data from the current eruption (Lisowski and others, this volume, chap. 15). The average volume percent groundmass of the 2004–5 dacite is 53.5 (Pallister and others, this volume, chap. 30; Rutherford and Devine, this volume, chap. 31). As such, it is a reasonable approximation of the rhyolitic melt fraction of the current dacite before its ascent and eruption from a shallow reservoir depth of 5.2 km (130 MPa)—the median of the 4.8–5.6-km depth range (120–140 MPa) where the dacite last equilibrated. This is the basis for the melt mass case corresponding to a melt fraction of 53.5 vol. percent in table 3. Accordingly, we have taken our results for all DEM dates obtained above (fig. 20) for dacite containing 70 vol. percent melt at 900°C, 220 MPa, and 8.6 km depth and repartitioned CO_2 and H_2O from melt to fluid to obtain a dacite with 53.5 vol. percent melt. To bring this dacite to the last equilibrium conditions within the shallow reservoir at 5.2 km (assuming a closed system), we used VolatileCalc to find the dissolved melt H_2O and CO_2 concentrations at 850°C and 130 MPa (fig. 21*A*) that—after further adjusting of H_2O and CO_2 partitioning between fluid and the 53.5-vol. percent melt phase—gave a fluid composition consistent with the X_{H_2O} and X_{CO_2} predicted by the model (fig. 21*B*). This iterative process consistently gave a melt H_2O concentration of ~4.4 wt. percent and an associated melt CO_2 concentration of ~37 ppm (fig. 21*A*) for each DEM date. The coexisting fluid composition is X_{H_2O} = ~0.96 and X_{CO_2} = ~0.04 (fig. 21*B*), consistent with experimental results of Rutherford and Devine (this volume, chap. 31) that indicate the X_{H_2O} of coexisting fluid would be close to 1.0 in the shallower part of the reservoir. These results also constrain the bulk dacite concentrations of CO_2 and H_2O—that is, fluid plus melt amounts of CO_2 and H_2O as mass fractions of the dacite—at average values of 1,167 ppm and 3.1 wt. percent, respectively, for the ten 2005 DEM dates. The corresponding average bulk dacite S concentration calculated from the cumulative SO_2 emissions (fig. 8; table 2) is 90 ppm for the 10 DEM dates.

The fluid content results for all the DEM dates range from 10.11 to 10.85 vol. percent (fig. 22); again, there is a tight grouping of steady fluid content for the ten 2005 DEM dates—10.63 to 10.85 vol. percent with an average 10.72 vol. percent. The large increase in the average volume percent fluid content from 1.23 to 10.72 vol. percent in going from 8.6 km to 5.2 km depth reflects the crystallization of melt (from 70 vol. percent melt to 53.5 vol. percent melt) and the decreased solubility of H_2O and CO_2 in rhyolite melt at lower pressure; it also includes the effect of fluid expansion as the pressure drops from 220 MPa to 130 MPa. The fluid expansion factor confounds comparisons of fluid content of magmas from different depths. This confusion is avoided by using mass units, which do

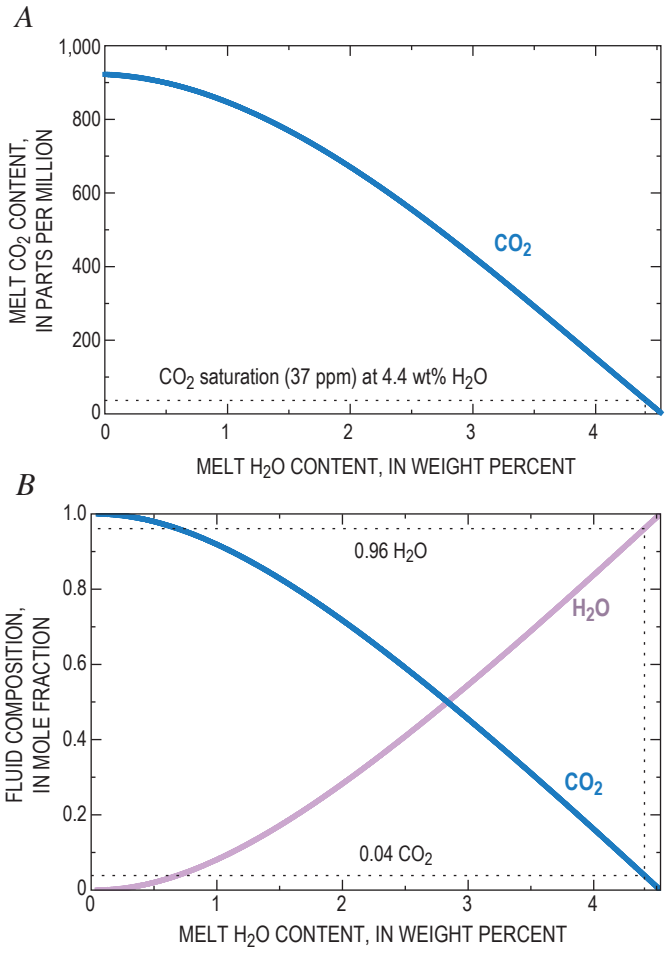

Figure 21. Concentration of CO_2 in hydrous rhyolitic melt and coexisting fluid composition at 130 MPa and 850°C (Newman and Lowenstern, 2002). *A*, Solubility of CO_2 (solid blue curve) in hydrous rhyolite melt with a range of water concentrations. Dotted lines indicate a CO_2 saturation limit of 37 ppm for rhyolitic melt containing 4.4 wt. percent H_2O. Melt H_2O content is total H_2O—that is, OH and molecular H_2O. *B*, Mole fraction concentrations of H_2O and CO_2 (solid curves) in fluids coexisting with hydrous rhyolitic melts over a range of water concentrations. Dotted lines indicate fluid composition of 0.96 X_{H_2O} and 0.04 X_{CO_2} coexisting with rhyolitic melt containing 4.4 wt. percent water.

not reflect fluid expansion; in the present case, the steady fluid content at 5.2 km depth ranges from 1.22 to 1.25 wt. percent and averages 1.23 wt. percent. Despite the relatively shallow depth, these results are still significantly smaller than Wallace's ≥3 wt. percent fluid content for the May 18 dacite at 8.6 km depth and on the low end of his 1–6 wt. percent range for deeper intermediate to silicic magmas involved in explosive volcanism (Wallace, 2001, 2003). These results further confirm the flat-magma hypothesis for the 2004–5 dacite.

We have assumed closed-system degassing with respect to the excess-volatile fluid phase's mobility in magma at depth. The steady excess-volatile fluid content of ~1.23 wt. percent calculated for the dacite at 5.2 km throughout 2005 is consistent with this assumption. Equilibrium (^{210}Pb)/(^{226}Ra) values reported for dacite erupted in 2004–5 (Reagan and others, this volume, chap. 37) also support closed-system degassing. Unlike those of the 1980 lava and tephra (Berlo and others, 2004), (^{210}Pb)/(^{226}Ra) values of the 2004–5 dacite were not affected by continuous open flow of fluid carrying ^{222}Rn from depth in sufficient amount or for sufficient duration to disturb secular equilibrium and generate ^{210}Pb deficits or excesses (Reagan and others, this volume, chap. 37); in our view, this reflects the depletion of excess volatiles compared to 1980 dacite. However, to explain the Li enrichment unique to plagioclase phenocrysts of the October 2004 dacite, Kent and others (2007) propose preferential partitioning of Li from deep melt into aqueous fluid migrating to the uppermost part of the magma chamber at 4.5 km, about 1 year before eruption; they argue that at this depth, which corresponds to 110 MPa (Williams and others, 1987), the fluid unmixed into a low-density vapor and a Li-rich brine that fostered the enrichment of Li in what became the October 2004 dacite's plagioclase phenocrysts. We suggest that Li in the dacite magma is partitioned preferentially into the accompanying excess-volatile fluid and that the Li-enriched plagioclase phenocrysts resulted when that fluid unmixed a Li-rich brine as the dacite ascended from 5.2 km to 4.5 km, where the magma stalled for several months before final ascent to the surface at the start of the eruption.

Ascent Degassing

We carried out calculations like those described above for the current dacite to model its closed-system degassing at 850°C during ascent from shallow reservoir depths. The calculations began at 5.2 km (130 MPa) and terminated at 0.47–0.95 km (10–20 MPa) where melt of the 1980s lava-dome eruptions crystallized extensively to groundmass (Blundy and Cashman, 2001). Figure 23 shows the fluid content, fluid composition, and melt H_2O and CO_2 concentrations of the dacite with ascent depth. We evaluated these variables for all DEM dates at each pressure of calculation and then correlated results to appropriate depths (Williams and others, 1987). The curves of figure 23 employ the average values of the ten 2005 DEM dates, which agreed within 5 percent.

Figure 23*A* shows the fluid content of the 2004–5 dacite during ascent; the fluid content of current dacite at 8.6 km and that of the May 18, 1980, dacite (Wallace, 2003) are included for comparison. The fluid content of the ascending 2004–5 dacite ranges from 10.7 vol. percent at the last equili-

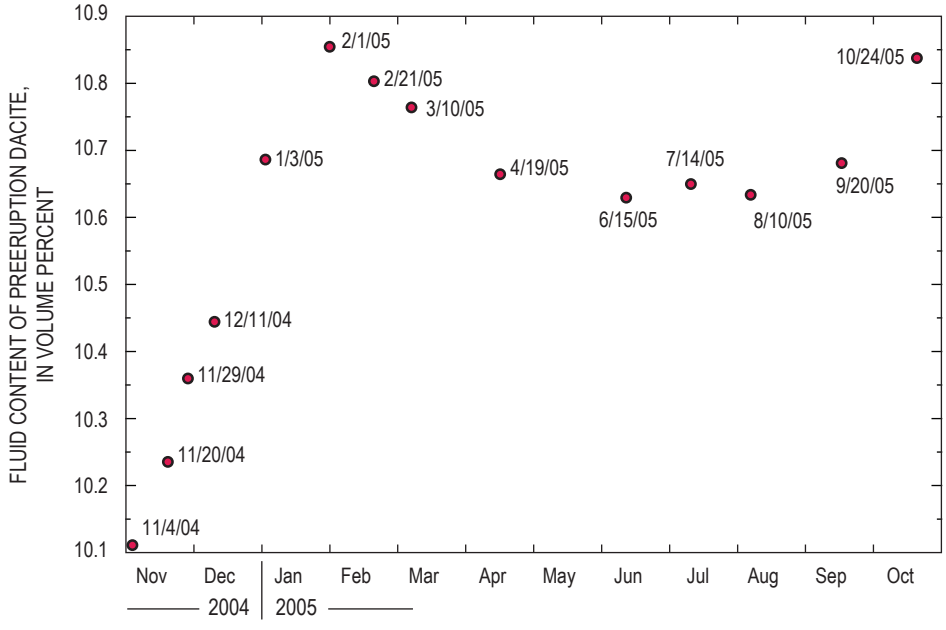

Figure 22. Fluid content of dacite at 850°C and 130 MPa (5.2 km) calculated as described in the text for 14 DEM dates in 2004–5.

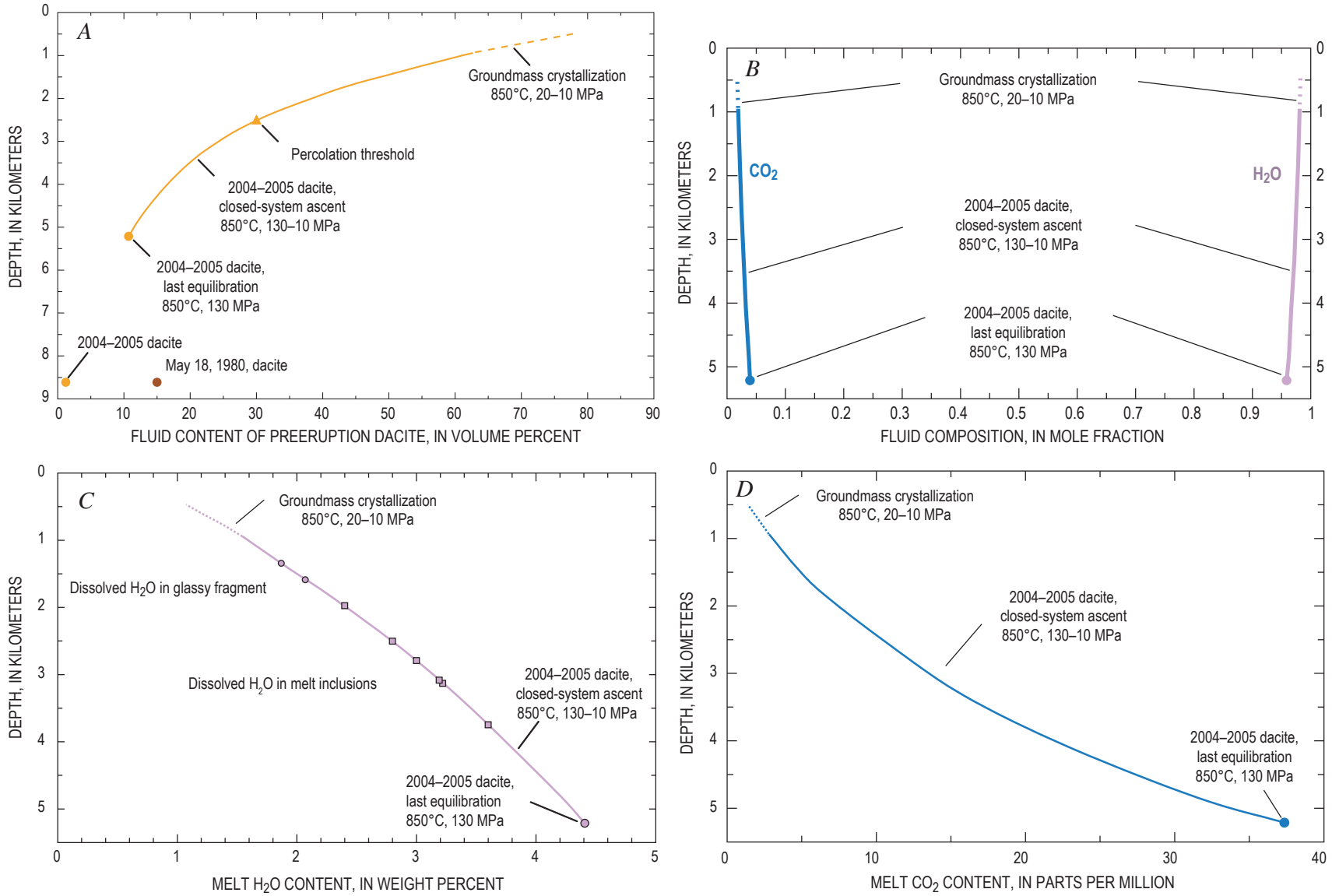

Figure 23. Closed-system ascent of 2004–2005 dacite from 5.2-km depth of last equilibration at 850°C and 130 MPa before eruption (Rutherford and Devine, this volume, chap. 31) to 0.47–0.95-km depth range of groundmass crystallization at 10–20 MPa (Blundy and Cashman, 2001). *A*, Fluid content (exolved fluid phase) of 2004–2005 dacite during ascent, and fluid content of 2004–2005 dacite and May 18, 1980, dacite (Wallace, 2003) at 8.6 km as discussed in the text. *B*, H_2O-CO_2 fluid composition of 2004–2005 dacite during ascent. *C*, Dissolved H_2O in melt of 2004–2005 dacite during ascent; dissolved H_2O in six melt inclusions (filled squares) with highest observed H_2O concentrations (Pallister and others, this volume, chap. 30; Blundy and others, this volume, chap. 33); and dissolved H_2O in a rare glassy fragment (filled circles) of October 2004 dacite sample SH304 (Pallister and others, 2005). *D*, Dissolved melt CO_2 concentration of 2004–2005 dacite during ascent.

bration depth to 60–80 vol. percent at depths of groundmass crystallization. The corresponding fluid composition of 2004–5 dacite during ascent (fig. 23*B*) is H_2O rich with X_{H_2O} always >0.96 and reaching 0.98 at the stage of groundmass crystallization. Extrapolating the compositional trends to near-surface conditions indicates that H_2O forms about 99 percent (molar basis) of the magmatic gases emitted to the atmosphere, whereas the monitored gases CO_2 and SO_2 account for only about 1 percent of the emitted magmatic gases. The implied magmatic $H_2O/(CO_2+SO_2)$ of ~99 is consistent with the value of 113 measured by open-path Fourier-transform infrared spectroscopy (Edmonds and others, this volume, chap. 27) on gas emissions from the new dome on August 31, 2005, considering that dome gases are likely to contain a meteoric component in addition to the magmatic component of water. Our CO_2 and SO_2 emission-rate data thus allow calculation of expected magmatic H_2O emission rates during 2004–5; the expected magmatic H_2O emission rates range from ~7 kt/d to ~100 kt/d with an estimated median of ~30 kt/d. We estimate cumulative H_2O production through 2005 at ~10 Mt from the cumulative production of CO_2 and SO_2.

The concentration of H_2O—that is, total OH and molecular H_2O—dissolved in the melt of the 2004–5 dacite ranges during ascent from the 4.4 wt. percent of last equilibration in the reservoir at 5.2 km to about 1.1–1.5 wt. percent at the conditions of groundmass crystallization (fig. 23*C*). The ascent curve for H_2O dissolved in melt indicates last equilibration depths of about 1.3–1.6 km for two measurements of H_2O concentration by Fourier-transform infrared spectrometry on a rare glassy fragment found in the October 2004 dacite sample SH304 (Pallister and others, 2005). Melt inclusions in the current dacite contain 0.0–3.6 wt. percent H_2O (Pallister and others, this volume, chap. 30; Blundy and others, this volume, chap. 33). The six highest melt-inclusion H_2O concentrations range from 2.4 to 3.6 wt. percent, corresponding to depths of only 2.0–3.7 km on the ascent curve for H_2O (fig. 23*C*). These results corroborate petrologic findings indicating that the melt inclusions provide no data on the volatile content of preeruption melt, apparently because slow ascent and eruption caused rupturing and (or) crystallization of virtually all melt inclusions, as suggested by their frequent mafic-mineral hosts, high crystallinity (≥70 percent), and variable SiO_2 concentrations (in this volume: Pallister and others, chap. 30; Rutherford and Devine, chap. 31; Blundy and others, chap. 33). Alternative explanations of the low melt-inclusion H_2O concentrations—for example, that they formed during ascent from 5.2 km, or that the source magma at 5.2 km depth was relatively dry (<4 wt. percent H_2O, which would imply X_{H_2O} <0.84)—are implausible in view of petrologic evidence. The concentration of CO_2 dissolved in the melt during ascent ranges from 37 ppm at the last equilibration in the reservoir at 5.2 km to about 1.3–2.9 ppm at the conditions of groundmass crystallization (fig. 23*D*).

The percolation threshold of 30 vol. percent indicated at ~2.5 km (fig. 23*A*) is a first-order approximation of the depth beyond which further ascent causes interconnected bubbles to increasingly dominate in overall degassing, ultimately transitioning to open-system degassing (Mueller and others, 2005). Melt concentrations of H_2O and CO_2 at the percolation threshold are about 2.8 wt. percent and 10 ppm, respectively, and the associated fluid composition is H_2O rich (X_{H_2O} = 0.975). The transition to open-system degassing during ascent at some depth shallower than ~2.5 km is an important step in the mobilization and flow of the H_2O-rich volcanic gases. Measured H_2O/HCl ratios of gas emissions on August 31, 2005, are consistent with a transition to open-system degassing at depths of ~1 km and prevailing to the surface (Edmonds and others, this volume, chap. 27). Open flow of H_2O-rich volcanic gases during ascent and dome emplacement purged shallow dacite of other volatile elements, including the entrainment of 210Po (Reagan and others, this volume, chap. 37) and the loss of Li from melt and the margins of plagioclase phenocrysts in the October 2004 dacite (Kent and others, 2007).

Fluid H_2S/SO_2 During Ascent

The gas-emission data show that SO_2 is the main sulfur species emitted to the atmosphere during the 2004–5 eruption. However, SO_2 may not be the dominant sulfur gas species at depth, where increased pressure can strongly affect sulfur speciation. Gerlach and Casadevall (1986) proposed from thermodynamic calculations constrained by fumarole gas compositions that H_2S was the dominant sulfur gas in the 1980s dacite at depth, whereas SO_2 dominated at pressures less than 4 MPa (depths less than 0.2 km). They cited reports of high H_2S/SO_2 in Mount St. Helens plumes from explosive eruptions of 1980–1981 in which 35–100 percent of the sulfur was present as H_2S (Hobbs and others, 1982) and suggested that rapid release of gas from depth prevented full equilibration to low pressure and allowed high H_2S/SO_2 to persist. They further suggested that rapid unloading during explosive eruptions of magma with oxygen fugacity as much as 1 order of magnitude above the Ni-NiO (NNO) buffer could burden the atmosphere with significant H_2S, as well as SO_2, and that SO_2 might increase as the H_2S oxidized, because the lifetime of H_2S in the atmosphere is only ~1 day (Graedel, 1977). Subsequent examination of TOMS satellite measurements made once a day on stratospheric volcanic clouds showed higher SO_2 masses for the May 18, 1980, cloud from Mount St. Helens on the second day than on the first day after eruption (Bluth and others, 1995).

We have taken a different approach to that of Gerlach and Casadevall (1986) and used the reaction

$$SO_2 + H_2O = H_2S + 1.5\ O_2$$

to estimate the H_2S/SO_2 ratio of the fluid phase during ascent of the current dacite from its last equilibration depth to the surface. For this reaction, the molar H_2S/SO_2 ratio is given by

$$H_2S/SO_2 = (pX_{H_2O}/Kf_{O_2}^{1.5})(\gamma_{H_2O}\gamma_{SO_2}/\gamma_{H_2S}), \quad (2)$$

where p is the total pressure in bars (1,300 bars to 1 bar), X_{H_2O} is the mole fraction of H_2O in the fluid (0.96 to 0.99, fig. 23*C*), K is the reaction equilibrium constant of $10^{20.03}$ at 850°C (HSC Chemistry for Windows v. 5.1), f_{O_2} is the current dacite's oxygen fugacity of $10^{-12.29}$ bar at 850°C (Pallister and others, this volume, chap. 30), and γ_i terms are dimensionless fugacity coefficients correcting for the nonideality of H_2O, SO_2, and H_2S. Fugacity coefficients from the MRK equation of state (Holloway, 1977, 1981), the corresponding state equation of Shi and Saxena (1992), and the ideal gas assumption ($\gamma_i = 1$) give H_2S/SO_2 results that agree within 10 percent, consistent with the relatively low-pressure, high-temperature conditions. The results confirm that H_2S is the dominant sulfur gas at depths >0.2 km (fig. 24), as in the 1980s (Gerlach and Casadevall, 1986); the H_2S/SO_2 ratio is >40 at the last equilibration depth in the shallow reservoir (5.2 km) and 3.3–6.5 in the depth range of groundmass crystallization (0.47 to 0.95 km). Compared to the explosive eruptions of the early 1980s, the slow ascent of magma from depth in the present eruption favors a closer approach to equilibrium with more complete conversion of H_2S to SO_2—consistent with the generally low H_2S emissions of the current eruption. Nevertheless, field crews often reported strong intermittent H_2S odor, especially after the early steam-and-ash events, and H_2S odor was reported by an airborne observer downwind of the volcano during and immediately after the first explosion of the eruption on October 1, 2004. These reports may be the result of rapid release of H_2S from depth. However, we cannot rule out an alternative H_2S origin by scrubbing and hydrolysis of SO_2, as discussed above, for the early days of the eruption in 2004.

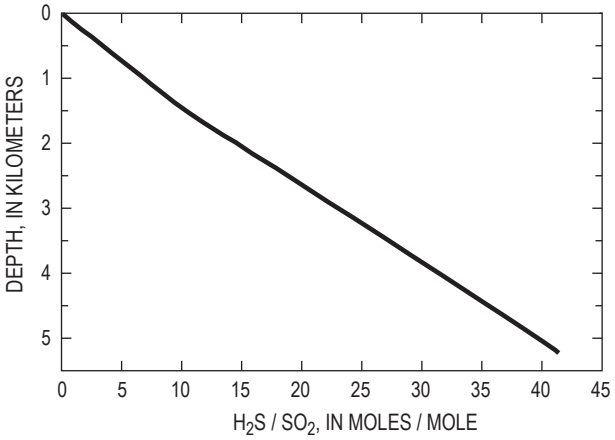

Figure 24. Calculated fluid H_2S/SO_2 of 2004–2005 dacite at 850°C ascending from the 5.2-km depth (130 MPa) of last equilibration in the shallow reservoir to the surface (0.1 MPa), as described in the text.

Excess Sulfur

The existence of an excess sulfur problem, although clear in the 1980s cycle of volcanism at Mount St. Helens (Gerlach and McGee, 1994), is problematic in the 2004–5 eruption. Assuming that the cumulative SO_2 emissions (table 2; fig. 8) for the DEM dates derived entirely from the melt fraction of the dacite prior to ascent implies a melt S concentration of 192 ppm at 5.2 km depth. The rupturing and high crystallinity of virtually all melt inclusions and the below-detection-limit sulfur concentrations of most melt inclusions and matrix glasses (Pallister and others, this volume, chap. 30), however, prevent the use of glass measurements to constrain the preeruption melt sulfur concentration of the current dacite prior to ascent from 5.2 km, thus precluding comparisons with the 192-ppm figure. Whether or not the preeruption melt sulfur concentration at 5.2 km depth accounts for the 2004–5 SO_2 emissions is therefore presently irresolvable, as is the question of excess sulfur for the 2004–5 eruption. The alternative source of the SO_2 emissions—that is, the fluid fraction of the dacite at 5.2 km—thus remains viable; this option would require a mole-fraction S concentration in the fluid (X_S) of only 0.004 prior to ascent (recall that the fluid X_{H_2O} and X_{CO_2} at 5.2 km are about 0.96 and 0.04, respectively). Moreover, experimental studies (Keppler, 1999) on haplogranitic melt at 850°C, 200 MPa, and f_{O_2} of 0.5 log units above the Ni-NiO buffer (NNO + 0.5)—close to the current dacite's f_{O_2} of NNO + ~1 (Pallister and others, this volume, chap. 30)—give fluid/melt partition coefficients for S of 47±4. These results strongly favor excess sulfur in the fluid fraction of the dacite at 5.2 km as the main source of the SO_2 emissions.

Concluding Remarks

The gas emissions of the 2004–5 eruption of Mount St. Helens provide no compelling evidence that gas-rich "new" magma was introduced into the reservoir during the months just prior to or since the onset of activity in September 2004, although additions of gas-poor new magma cannot be ruled out. The gas emissions are instead indicative of a flat source magma markedly depleted in excess volatiles compared to the May 18, 1980, dacite and the intermediate and silicic magmas commonly involved in explosive volcanism. However, the flat dacite of this eruption contains rhyolitic melt with appreciable dissolved water (4.4 wt. percent) despite its depletion in excess volatiles. It remains unclear whether flat dacite of this sort can give rise to large and violent explosive eruptions. The flat dacite has not done so in the present case, but this fact begs the question of how dependent explosive volcanism involving intermediate and silicic magma is on the magnitude of the excess-volatile load.

The 2004–5 gas emissions are plausibly compatible with 1980–86 dome-building magma left over in the reservoir and (or) with gas-poor new magma that entered the reservoir since 1986. Petrologic evidence favors the introduction of new magma (Pallister and others, this volume, chap. 30), but why is this new magma so gas poor compared to the May 18, 1980, magma? Perhaps the new magma was initially depleted in excess volatiles, or it may have mixed with a large amount of leftover 1980–86 magma already greatly depleted in exsolved volatiles. Alternatively, the new magma may simply have lost most of its excess-volatile load by fluid escape while stored at shallow reservoir depths long before the events of September 2004. The degassing of CO_2 measured on June 22, 1998, may represent the product of such fluid escape during a short period of seismicity accompanying recharge of the shallow reservoir. Although this is the strongest evidence of post-1986 fluid escaping and reaching the surface, we cannot rule out the possibility that fluid escaped from the shallow reservoir at other times since 1986 and was captured by hydrothermal fluid at depth or scrubbed by surficial water (Shevenell and Goff, 1993); the large increase of HCO_3^- in the waters of thermal springs at Loowit and Step canyons since 1994 (Bergfeld and others, this volume, chap. 25) may be the result of these processes.

The small load of excess volatiles in the 2004–5 dacite was an important factor in making it possible for scrubbing to shut down and strongly reduce gas emissions to the atmosphere in the period of unrest and the early stage of the eruption. The 2004–5 eruption affirms several implications of scrubbing for assessment of volcano hazards by volcanic gas monitoring: scrubbing can mask shallow magmatic degassing and thus severely restrict gas-emission monitoring as a volcano hazards assessment tool; scrubbing and its masking effects are most effective in the early stages of unrest; no great solace should be taken from low SO_2 emission rates during periods of unrest; early monitoring of CO_2 should accompany early SO_2 monitoring; the monitoring of CO_2, SO_2, and H_2S can track the drying out of a volcano and help distinguish the effects of gas scrubbing and permeability sealing on emissions; and emissions of CO_2 and H_2S in the early stages of unrest, when SO_2 and emissions are absent or trivial, should not be regarded as merely the degassing of hydrothermal fluid, as they can reflect significant shallow magmatic degassing combined with the effects of scrubbing.

Acknowledgments

We are indebted to the following, all of whom made valuable contributions to this paper by sharing ideas, observations and data: Roger Denlinger, Dan Dzurisin, Marie Edmonds, Mike Lisowski, Larry Mastin, John Pallister, Kelly Russell, Steve Schilling, Carl Thornber, and Paul Wallace. Our special thanks to Jeff Sutton for help with instrumentation and early monitoring flights, and to Larry Mastin and John Pallister for technical reviews. Finally, we acknowledge the support of the U.S. Geological Survey Volcano Hazards Program.

References Cited

Anderson, C.H., Jr., Behrens, C.J., Floyd, G.A., and Vining, M.R., 1998, Crater firn of Mount St. Helens, Washington: Journal of Cave Karst Studies, v. 60, p. 44–50.

Bergfeld, D., Evans, W.C., McGee, K.A., and Spicer, K.R., 2008, Pre- and post-eruptive investigations of gas and water samples from Mount St. Helens, Washington, 2002 to 2005, chap. 25 *of* Sherrod, D.R., Scott, W.E., and Stauffer, P.H., eds., A volcano rekindled; the renewed eruption of Mount St. Helens, 2004–2006: U.S. Geological Survey Professional Paper 1750 (this volume).

Berlo, K., Blundy, J., Turner, S., Cashman, K., Hawkesworth, C., and Black, S., 2004, Geochemical precursors to volcanic activity at Mount St. Helens, USA: Science, v. 306, p. 1167–1169.

Blundy, J., and Cashman, K., 2001, Ascent-driven crystallisation of dacite magmas at Mount St. Helens, 1980–1986: Contributions to Mineralogy and Petrology, v. 140, no. 6, p. 631–650, doi:10.1007/s004100000219.

Blundy, J., and Cashman, K., 2005, Rapid decompression-driven crystallization recorded by melt inclusions from Mount St. Helens volcano: Geology, v. 33, no. 10, p. 793–796, doi:10.1130/G21668.1.

Blundy, J., Cashman, K.V., and Berlo, K., 2008, Evolving magma storage conditions beneath Mount St. Helens inferred from chemical variations in melt inclusions from the 1980–1986 and current (2004–2006) eruptions, chap. 33 *of* Sherrod, D.R., Scott, W.E., and Stauffer, P.H., eds., A volcano rekindled; the renewed eruption of Mount St. Helens, 2004–2006: U.S. Geological Survey Professional Paper 1750 (this volume).

Bluth, G.J.S., Scott, C.J., Sprod, I.E., Schnetzler, C.C., Krueger, A.J., and Walter, L.S., 1995, Explosive emissions of sulfur dioxide from the 1992 Crater Peak eruptions, Mount Spurr volcano, Alaska, *in* Keith, T., ed., The 1992 eruptions of Crater Peak vent, Mount Spurr volcano, Alaska: U.S. Geological Survey Bulletin 2139, p. 37–45.

Caltabiano, T., Guiduzzi, G., Leuzzi, S., and Romano, R., 1992, Helicopter borne COSPEC SO_2 flux measurement: Acta Vulcanologica, v. 2, p. 95–98.

Casadevall, T.J., Johnston, D.A., Harris, D.M., Rose, W.I., Malinconico, L.L., Stoiber, R.E., Bornhorst, T.J., Williams, S.N., Woodruff, L., and Thompson, J.M., 1981, SO_2 emission rates at Mount St. Helens from March 29 through December, 1980, *in* Lipman, P.W., and Mullineaux, D.L., eds., The 1980 eruptions of Mount St. Helens, Washington: U.S. Geological Survey Professional Paper 1250, p. 193–200.

Casadevall, T.J., Johnston, D.A., Rose, W.I., Gerlach, T.M., Ewert, J., Wunderman, R., and Symonds, R., 1983, Gas

emissions and the eruptions of Mount St. Helens through 1982: Science, v. 221, p. 1383–1385.

Cashman, K.V., 1992, Groundmass crystallization of Mount St. Helens dacite, 1980–1986—a tool for interpreting shallow magmatic processes: Contributions to Mineralogy and Petrology, v. 109, no. 4, p. 431–449, doi:10.1007/BF00306547.

Cashman, K.V., and Taggert, J.E., 1983, Petrologic monitoring of 1981 and 1982 eruptive products from Mount St. Helens: Science, v. 221, no. 4618, p. 1385–1387.

Cashman, K.V., Thornber, C.R., and Pallister, J.S., 2008, From dome to dust; shallow crystallization and fragmentation of conduit magma during the 2004–2006 dome extrusion of Mount St. Helens, Washington, chap. 19 *of* Sherrod, D.R., Scott, W.E., and Stauffer, P.H., eds., A volcano rekindled; the renewed eruption of Mount St. Helens, 2004–2006: U.S. Geological Survey Professional Paper 1750 (this volume).

Cooper, K.M., and Donnelly, C.T., 2008, ^{238}U-^{230}Th-^{226}Ra disequilibria in dacite and plagioclase from the 2004–2005 eruption of Mount St. Helens, chap. 36 *of* Sherrod, D.R., Scott, W.E., and Stauffer, P.H., eds., A volcano rekindled; the renewed eruption of Mount St. Helens, 2004–2006: U.S. Geological Survey Professional Paper 1750 (this volume).

Crafford, T.C., 1975, SO_2 emission of the 1974 eruption of Volcán Fuego, Guatemala: Bulletin Volcanologique, v. 39, p. 536–556.

Doukas, M.P., 2002, A new method for GPS-based wind speed determinations during airborne volcanic plume measurements: U.S. Geological Survey Open-File Report 02–395, 13 p.

Doukas, M.P., and Gerlach, T.M., 1995, Sulfur dioxide scrubbing during the 1992 eruption of Crater Peak, Mount Spurr, Alaska, *in* Keith, T., ed., The 1992 eruptions of Crater Peak vent, Mount Spurr volcano, Alaska: U.S. Geological Survey Bulletin 2139, p. 47–57.

Edmonds, M., McGee, K.A., and Doukas, M.P., 2008, Chlorine degassing during the lava dome-building eruption of Mount St. Helens, 2004–2005, chap. 27 *of* Sherrod, D.R., Scott, W.E., and Stauffer, P.H., eds., A volcano rekindled; the renewed eruption of Mount St. Helens, 2004–2006: U.S. Geological Survey Professional Paper 1750 (this volume).

Elias, T., Sutton, A.J., Oppenheimer, C., Horton, K.A., Garbeil, H., Tsanev, V., McGonigle, A.J.S., and Williams-Jones, G., 2006, Comparison of COSPEC and two miniature ultraviolet spectrometer systems for SO_2 measurements using scattered sunlight: Bulletin of Volcanology, v. 68, p. 313–322.

Evans, W.C., van Soest, M.C., Mariner, R.H., Hurwitz, S., Wicks, C.W., Jr., and Schmidt, M.E., 2004, Magmatic intrusion west of Three Sisters, central Oregon, USA: The perspective from spring geochemistry: Geology, v. 32, no. 1, p. 69–72.

Galle, B., Oppenheimer, C., Geyer, A., McGonigle, A.J.S., Edmonds, M., and Horrocks, L., 2002, A miniaturized ultraviolet spectrometer for remote sensing of SO_2 fluxes—a new tool for volcano surveillance: Journal of Volcanology and Geothermal Research, v. 119, p. 241–254.

Gerlach, T.M., and Casadevall, T.J., 1986, Fumarole emissions at Mount St. Helens volcano, June 1980 to October 1981—degassing of a magma-hydrothermal system: Journal of Volcanology and Geothermal Research, v. 28, nos. 1–2, p. 141–160, doi:10.1016/0377-0273(86)90009-0.

Gerlach, T.M., and McGee, K.A., 1994, Total sulfur dioxide emissions and pre-eruption vapor-saturated magma at Mount St. Helens, 1980–88: Geophysical Research Letters, v. 21, no. 25, p. 2833–2836, doi:10.1029/94GL02761.

Gerlach, T.M., Delgado, H., McGee, K.A., Doukas, M.P., Venegas, J.J., and Cardenas, L., 1997, Application of the LI-COR CO_2 analyzer to volcanic plumes—a case study, Volcán Popocateptl, Mexico, June 7 and 10, 1995: Journal of Geophysical Research, v. 102, p. 8005–8019.

Gerlach, T.M., Doukas, M.P., McGee, K.A., and Kessler, R., 1999, Airborne detection of diffuse carbon dioxide at Mammoth Mountain, California: Geophysical Research Letters, v. 26, 3661–3664.

Gerlach, T.M., McGee, K.A., and Doukas, M.P., 2005, Emission rates, pre-eruption gas saturation and ascent degassing during the 2004–2005 eruption of Mount St. Helens [abs.]: Eos (American Geophysical Union Transactions), v. 86, no. 52, Fall Meet. Suppl., Abstract V52B–07.

Glantz, S.A., 2005, Primer of biostatistics (5th ed.): New York, McGraw-Hill, 489 p.

Graedel, T.E., 1977, The homogeneous chemistry of atmospheric sulfur: Reviews of Geophysics and Space Physics, v. 15, p. 421–428.

Harris, D.M., Sato, M., Casadevall, T.J., Rose, W.I., and Bornhorst, T.J., 1981, Emission rates of CO_2 from plume measurements, *in* Lipman, P.W., and Mullineaux, D.L., eds., The 1980 eruptions of Mount St. Helens, Washington: U.S. Geological Survey Professional Paper 1250, p. 201–207.

Hobbs, P.V., Tuell, J.P., Hegg, D.A., Radke, L.F., and Eltgroth, M.W., 1982, Particles and gases in the emissions from the 1980–1981 volcanic eruptions of Mount St. Helens: Journal of Geophysical Research, v. 87, no. C12, p. 11062–11086.

Holloway, J.R., 1977, Fugacity and activity of molecular species in supercritical fluids, *in* Fraser, D., ed., Thermodynamics in Geology: Boston, D. Reidel, p. 161–181.

Holloway, J.R., 1981, Volatile interactions in magmas, *in* Newton, R.C., Navrotsky, A., and Wood, B.J., eds., Thermodynamics of Minerals and Melts: New York, Springer-Verlag, p. 273–293.

Horton, K.A., Williams-Jones, G., Garbeil, H., Elias, T., Sutton, A.J., Mouginis-Mark, P., Porter, J.N., and Clegg, S., 2006, Real-time measurement of volcanic SO_2 emissions: validation of a new UV correlation spectrometer (FLYSPEC): Bulletin of Volcanology, v. 68, p. 323–327.

Ingebritsen, S.E., Sherrod, D.R., and Mariner, R.H., 1989, Heat flow and hydrothermal circulation in the Cascade Range, north-central Oregon: Science, v. 243, p. 1458–1462.

Ingebritsen, S.E., Sherrod, D.R., and Mariner, R.H., 1992, Rate and patterns of groundwater flow in the Cascade Range volcanic arc, and the effect on subsurface temperatures: Journal of Geophysical Research, v. 97, no. B4, p. 4599–4627.

Ingebritsen, S.E., Mariner, R.H., and Sherrod, D.R., 1994, Hydrothermal systems of the Cascade Range, north-central Oregon: U.S. Geological Survey Professional Paper 1044L, 86 p.

James, E.R., Manga, M., and Rose, T.P., 1999, CO_2 degassing in the Oregon Cascades: Geology, v. 27, no. 9, p. 823–826.

Kent, A.J.R., Blundy, J., Cashman, K.V., Cooper, K.M., Donnelly, C., Pallister, J.S., Reagan, M., Rowe, M.C., and Thornber, C.R., 2007, Vapor transfer prior to the October 2004 eruption of Mount St. Helens, Washington: Geology, v. 35, no. 3, p. 231–234, doi:10.1130/G22809A.1.

Keppler, H., 1999, Experimental evidence for the source of excess sulfur in explosive volcanic eruptions: Science, v. 284, p. 1652–1654.

Lisowski, M., Dzurisin, D., Denlinger, R.P., and Iwatsubo, E.Y., 2008, Analysis of GPS-measured deformation associated with the 2004–2006 dome-building eruption of Mount St. Helens, Washington, chap. 15 *of* Sherrod, D.R., Scott, W.E., and Stauffer, P.H., eds., A volcano rekindled; the renewed eruption of Mount St. Helens, 2004–2006: U.S. Geological Survey Professional Paper 1750 (this volume).

Liu, Y., Zhang, Y., and Behrens, H., 2005, Solubility of H_2O in rhyolite melts at low pressures and a new empirical model for mixed H_2O-CO_2 solubility in rhyolitic melts: Journal of Volcanology and Geothermal Research, v. 143, p. 219–235.

Malinconico, L.L., 1979, Fluctuations in SO_2 emission during recent eruptions of Etna: Nature, v. 278, p. 43–45.

Mastin, L.G., Roeloffs, E., Beeler, N.M., and Quick, J.E., 2008, Constraints on the size, overpressure, and volatile content of the Mount St. Helens magma system from geodetic and dome-growth measurements during the 2004–2006+ eruption, chap. 22 *of* Sherrod, D.R., Scott, W.E., and Stauffer, P.H., eds., A volcano rekindled; the renewed eruption of Mount St. Helens, 2004–2006: U.S. Geological Survey Professional Paper 1750 (this volume).

McGee, K.A., 1992, The structure, dynamics, and chemical composition of noneruptive plumes from Mount St. Helens, 1980–88: Journal of Volcanology and Geothermal Research, v. 51, p. 269–282.

McGee, K.A., and Casadevall, T.J., 1994, A compilation of sulfur dioxide and carbon dioxide emission-rate data from Mount St. Helens during 1980–88: U.S. Geological Survey Open-File Report 94–212, 24 p.

McGee, K.A., and Sutton, A.J., 1994, Eruptive activity at Mount St. Helens, Washington, USA, 1984–1988—a gas geochemistry perspective: Bulletin of Volcanology, v. 56, nos. 6–7, p. 435–446.

McGee, K.A., Doukas, M.P., and Gerlach, T.M., 2001, Quiescent hydrogen sulfide and carbon dioxide degassing from Mount Baker, Washington: Geophysical Research Letters, v. 28, p. 4479–4483.

Moran, S.C., 1994, Seismicity at Mount St. Helens, 1987–1992—evidence for repressurization of an active magmatic system: Journal of Geophysical Research, v. 99, no. B3, p. 4341–4354, doi:10.1029/93JB02993.

Moran, S.C., Malone, S.D., Qamar, A.I., Thelen, W.A., Wright, A.K., and Caplan-Auerbach, J., 2008, Seismicity associated with renewed dome building at Mount St. Helens, 2004–2005, chap. 2 *of* Sherrod, D.R., Scott, W.E., and Stauffer, P.H., eds., A volcano rekindled; the renewed eruption of Mount St. Helens, 2004–2006: U.S. Geological Survey Professional Paper 1750 (this volume).

Mueller, S., Melnik, O., Spieler, O., Scheu, B., and Dingwell, D.B., 2005, Permeability and degassing of dome lavas undergoing rapid decompression—an experimental determination: Bulletin of Volcanology, v. 67, no. 6, p. 526–538.

Newman, S., and Lowenstern, J.A., 2002, VolatileCalc—a silicate melt-H_2O-CO_2 solution model written in Visual Basic for excel®: Computers and Geosciences, v. 28, no. 5, p. 597–604, doi:10.1016/S0098-3004(01)00081-4.

Pallister, J.S., Reagan, M., and Cashman, K., 2005, A new eruptive cycle at Mount St. Helens?: Eos (American Geophysical Union Transactions), v. 86, no. 48, p. 499–500, doi:10.1029/2005EO480006.

Pallister, J.S., Thornber, C.R., Cashman, K.V., Clynne, M.A., Lowers, H.A., Mandeville, C.W., Brownfield, I.K., and Meeker, G.P., 2008, Petrology of the 2004–2006 Mount St. Helens lava dome—implications for magmatic plumbing and eruption triggering, chap. 30 *of* Sherrod, D.R., Scott, W.E., and Stauffer, P.H., eds., A volcano rekindled; the renewed eruption of Mount St. Helens, 2004–2006: U.S. Geological Survey Professional Paper 1750 (this volume).

Reagan, M.K., Cooper, K.M., Pallister, J.S., Thornber, C.R., and Wortel, M., 2008, Timing of degassing and plagioclase

growth in lavas erupted from Mount St. Helens, 2004–2005, from ^{210}Po-^{210}Pb-^{226}Ra disequilibria, chap. 37 *of* Sherrod, D.R., Scott, W.E., and Stauffer, P.H., eds., A volcano rekindled; the renewed eruption of Mount St. Helens, 2004–2006: U.S. Geological Survey Professional Paper 1750 (this volume).

Rose, T.P., and Davisson, M.L., 1996, Radiocarbon in hydrologic systems containing dissolved magmatic carbon dioxide: Science, v. 273, p. 1367–1370.

Rutherford, M.J., 1993, Experimental petrology applied to volcanic processes: Eos (American Geophysical Union Transactions), v. 74, no. 5, p. 49 and 55.

Rutherford, M.J., and Devine, J.D., III, 2008, Magmatic conditions and processes in the storage zone of the 2004–2006 Mount St. Helens dacite, chap. 31 *of* Sherrod, D.R., Scott, W.E., and Stauffer, P.H., eds., A volcano rekindled; the renewed eruption of Mount St. Helens, 2004–2006: U.S. Geological Survey Professional Paper 1750 (this volume).

Rutherford, M.J., Sigurdsson, H., Carey, S., and Davis, A., 1985, The May 18, 1980, eruption of Mount St. Helens, 1. Melt composition and experimental phase equilibria: Journal of Geophysical Research, v. 90, no. B4, p. 2929–2947.

Schilling, S.P., Thompson, R.A., Messerich, J.A., and Iwatsubo, E.Y., 2008, Use of digital aerophotogrammetry to determine rates of lava dome growth, Mount St. Helens, Washington, 2004–2005, chap. 8 *of* Sherrod, D.R., Scott, W.E., and Stauffer, P.H., eds., A volcano rekindled; the renewed eruption of Mount St. Helens, 2004–2006: U.S. Geological Survey Professional Paper 1750 (this volume).

Scott, W.E., Sherrod, D.R., and Gardner, C.A., 2008, Overview of 2004 to 2006, and continuing, eruption of Mount St. Helens, Washington, chap. 1 *of* Sherrod, D.R., Scott, W.E., and Stauffer, P.H., eds., A volcano rekindled; the renewed eruption of Mount St. Helens, 2004–2006: U.S. Geological Survey Professional Paper 1750 (this volume).

Shevenell, L., and Goff, F., 1993, Addition of magmatic volatiles into the hot spring waters of Loowit Canyon, Mount St. Helens, Washington, USA: Bulletin of Volcanology, v. 55, no. 7, p. 489–503, doi:10.1007/BF00304592.

Shi, P., and Saxena, S.K., 1992, Thermodynamic modeling of the C-H-O-S fluid system: American Mineralogist, v. 77, p. 1038–1049.

Silver, L.A., Ihinger, P.D., and Stolper, E., 1990, The influence of bulk composition on the speciation of water in silicate glasses: Contributions to Mineralogy and Petrology, v. 104, p. 142–162.

Stoiber, R.E., and Jepsen, A., 1973, Sulfur dioxide contribution to the atmosphere by volcanoes: Science, v. 182, p. 577–578.

Stoiber, R.E., Williams, S.N., and Malinconico, L.L., 1980, Mount St. Helens, Washington, 1980, volcanic eruption—magmatic gas component during the first 16 days: Science, v. 208, p. 1258–1259.

Stoiber, R.E., Malinconico, L.L., and Williams, S.N., 1983, Use of the correlation spectrometer at volcanoes, *in* Tazieff, H., and Sabroux, J.C., eds., Forecasting volcanic events: Amsterdam, Elsevier, p. 425–444.

Symonds, R.B., Gerlach, T.M., and Reed, M.H., 2001, Magmatic gas scrubbing—implications for volcanic monitoring: Journal of Volcanology and Geothermal Research, v. 108, nos. 1–4, p. 303–341, doi:10.1016/S0377-0273(00)00292-4.

Thompson, J.M., 1990, Chemical data from thermal and nonthermal springs in Mount St. Helens National Monument, Washington: U.S. Geological Survey Open-File Report 90–690A, 16 p.

Wallace, P.J., 2001, Volcanic SO_2 emissions and the abundance and distribution of exsolved gas in magma bodies: Journal of Volcanology and Geothermal Research, v. 108, nos. 1–4, p. 85–106, doi:10.1016/S0377-0273(00)00279-1.

Wallace, P.J., 2003, From mantle to atmosphere—magma degassing, explosive eruptions, and volcanic volatile budgets, *in* De Vivo, B., and Bodnar, R.J., eds., Melt inclusions in volcanic systems—methods, applications and problems: Amsterdam, Elsevier, p. 105–128.

Williams, D.L., Abrams, G., Finn, C., Dzurisin, D., Johnson, D.J., and Denlinger, R., 1987, Evidence from gravity data for an intrusive complex beneath Mount St. Helens: Journal of Geophysical Research, v. 92, no. B10, p. 10207–10222.